Universal Fault-Tolerant SVPWM Strategy With Simplified Fault Diagnosis for Five-Phase PMSM Under Arbitrary Phase Single Open-Switch Fault

Xu Wang, *Member, IEEE*, Zhengmeng Liu, *Member, IEEE*, Qian Chen, *Senior Member, IEEE*, Wenxiang Zhao, *Senior Member, IEEE*, and Guohai Liu, *Senior Member, IEEE*

***Abstract*—The standard inverter topology of five-phase permanent magnet synchronous motor (PMSM) has weaker fault-tolerant capability than other complex drives. Additionally, traditional open-switch fault-tolerant strategies demand precise diagnosis methods involving numerous states of different phases and reconfiguration according to fault phase change. To enhance fault-tolerant algorithm applicability, a universal fault-tolerant space vector pulsewidth modulation (SVPWM) strategy without extra hardware is proposed to handle single open-switch fault for five-phase PMSM. The most significant innovation is to achieving fault-tolerant operation for arbitrary phase open-switch fault without requiring adjustments based on fault phase location. Owing to this, corresponding diagnosis process can be simplified. In diagnosis process, the positive and negative relationship of the third harmonic currents within faulty half cycle is adopted to obtain the overall diagnosis result without requiring precise identification. In fault-tolerant algorithm, postfault basic voltage vectors are first reconstructed based on switching state analysis. Then, to minimize the influence of harmonic subspace and improve SVPWM control precision, virtual voltage vectors are synthesized based on geometric meaning of basic voltage vectors. Furthermore, through establishing vector sets involving five phases and summarizing their intersection regions, universal virtual voltage vectors are determined. Finally, the effectiveness of proposed method is verified by experiments.**

***Index Terms*—Diagnosis, fault tolerant control, five-phase permanent magnet synchronous machine (PMSM), open-switch fault, space vector pulsewidth modulation (SVPWM), universal, virtual voltage vector.**

I. Introduction

MULTIPHASE permanent magnet synchronous motor (PMSM) exhibits promising potential for practical owing to its high efficiency, high power density, and high torque inertia ratio [1], [2], [3], [4]. In environments with stringent security and reliability requirements, it is imperative to detect and resolve faults promptly. Moreover, the system may need to operate with fault-tolerant capabilities. Due to the increase in the number of phases, the motor has a higher degree of freedom and is more flexible to control. Even in the case of fault, the motor can still operate stably [5], [6] by adjusting the control strategy reasonably according to fault types, such as open-circuit fault [7], [8] and short-circuit fault [9], [10]. Three-phase motor is the most common due to their simple structure and low cost; however, they exhibit significant torque fluctuations and limited fault tolerance. Six-phase and higher multiphase motors generally offer superior fault tolerance and reduced torque fluctuations, but their control systems are more complex and expensive. Five-phase motor occupies an intermediate position, providing a balanced compromise between performance, cost, and complexity, making it particularly valuable for research.

The inverter serves as the critical interface between energy flow and digital control in the motor system, rendering it susceptible to parasitic effects, crosstalk, and other interferences. Once open-switch fault occurs, the stator current will increase rapidly. If the fault is not addressed promptly, the motor temperature will rise sharply, potentially leading to motor damage and even secondary faults. This could result in the paralysis of the entire drive system, causing severe damage and considerable economic losses. In practical applications, it is impossible to allow the initial single power device fault to evolve into multiple power device faults, or even to the destruction of the entire motor system. Therefore, the most commonly discussed and studied fault type is the single open-switch fault [11], while multiple open-switch fault is an extension of fault-tolerant technology after maturity. Cui and Fan [12], Zhao et al. [13], and Zuo et al. [14], respectively, designed different kinds of inverter topologies and implements fault-tolerant operation through winding reconnection in a dual-inverter fed open-end winding three-phase PMSM. Du et al. [15] applied the concept of reconstructing inverter structure to open-end winding five-phase PMSM, similarly achieved by connecting the windings to the midpoint of the bus capacitor. However, the realization of these methods is attributed to the unique structure of the dual-inverter drive and the connecting mode of open winding motor, which is not universally applicable and unsuitable for the most common five-phase PMSM. For

Received 9 April 2025; revised 30 July 2025; accepted 27 August 2025. Date of publication 29 August 2025; date of current version 22 October 2025. This work was supported in part by the National Natural Science Foundation of China under Grant 52377054 and in part by the Senior Talent Fund of Jiangsu University under Grant 5501140009. Recommended for publication by Associate Editor M. Molinas. *(Corresponding author: Zhengmeng Liu.)*

The authors are with the School of Electrical and Information Engineering, Jiangsu University, Zhenjiang 212013, China, and also with the Jiangsu Key Laboratory of Drive and Intelligent Control for Electric Vehicle, Zhenjiang 212013, China (e-mail: 2112207013@stmail.ujs.edu.cn; lzm@ujs.edu.cn; chenqian0501@ujs.edu.cn; zwx@ujs.edu.cn; ghliu@ujs.edu.cn).

Color versions of one or more figures in this article are available at https://doi.org/10.1109/TPEL.2025.3604438.

Digital Object Identifier 10.1109/TPEL.2025.3604438

the common two-level inverter-fed PMSM, if five-phase six-leg inverter topology [16] is used, the entire bridge arm of the faulty phase will be removed and replaced with a new bridge arm. This approach does not differ from standard operational procedures and it merely offers a greater variety of alternative configurations. Most importantly, all the aforementioned methods are hardware-based fault-tolerant strategies, necessitating specific topologies and additional solid-state relays (SSR) or entire phase bridge arm. The supplementary hardware not only elevates the economic overhead but also potentially increases the likelihood of additional faults.

To intrinsically improve the reliability, fault-tolerant algorithms in software have been continuously developed. Zhou et al. [17] and Tian et al. [18] provided remedial strategies utilizing reduced-order transformation matrix for five-phase PMSM. But this method treats open-switch fault as open-phase fault and does not utilize the entire faulty phase bridge arm, which is neither cost-effective nor efficient. Tian et al. [19] introduced a new sensorless method by exploiting the freewheeling current to accommodate open-switch faults. However, it highly relies upon the parameters of the observer model and speed exhibits fluctuation. Sun et al. [20] and Huang et al. [21] injected extra currents to eliminate the torque ripples brought by faults but increases extra losses and instability of the system. Zhang et al. [22] proposed a postfault space voltage vectors reallocation strategy based on the mathematical analysis of the postfault space voltage vectors. However, it is only applicable to three-phase PMSM with a limited number of voltage vectors and cannot be directly extended to five-phase PMSM with a greater number of voltage vectors and an additional harmonic subspace.

Moreover, it is essential to emphasize that in practical applications, the principle of diagnosis first and fault-tolerance later should be adhered to. On one hand, these methods are usually developed based on precise identification of the fault location, which is not natural. At this time, it is imperative to utilize advanced diagnosis methods [23], [24], [25]. While these accurate diagnostic methods demonstrate high efficacy, numerous states of different phases require careful consideration, thereby rendering the entire diagnosis process complex and time-intensive. On the other hand, these traditional fault-tolerant strategies necessitate reconfiguration based on specific fault locations. For n-phase motors, at least n fault indices are required to provide comprehensive information and ensure seamless fault-tolerant operations. Consequently, the simplification of the diagnosis process and enhancement of the algorithm's universality become a top priority.

Yang et al. [26] proposed a universal natural fault-tolerant strategy for open-phase faults of multiphase motor. On this basis, Zhou et al. [27] designed universal five-phase fault-tolerant switching table for five-phase PMSM direct torque control (DTC). However, it is only suitable for open-phase fault. At present, there is absence of universal fault-tolerant strategy for open-switch fault due to its complex and variable characteristics. In addition, it is widely recognized that space vector pulsewidth modulation (SVPWM) offers superior advantages compared with DTC in the steady-state performance of the system, which is worth further application on open-switch fault.

In this article, a universal fault-tolerant SVPWM strategy with simplified fault diagnosis is proposed to realize arbitrary phase single open-switch fault-tolerant operation for five-phase PMSM. The contributions and novelties can be summarized as follows.

1) The entire system that encompasses both diagnosis and fault tolerance is more aligned with practical applications. No additional hardware investments can achieve economic cost savings. Then, no additional current injection and transformation matrix modification makes the software algorithm simpler.
2) The simplified open-switch diagnosis utilizing the third harmonic components of phase currents can match with universal fault-tolerant strategy, which necessitates only an overall assessment of the upper or lower tube, thereby reducing the diagnosis states and computation burden.
3) The synthesis of virtual voltage vectors according to mathematical principles and geometric meanings can maximally eliminate the influence of harmonic subspace. The modified SVPWM with the reallocation of vector acting time can accurately track the reference voltage and improve the steady-state performance.
4) Through analyzing the characteristics and summarizing the intersection region of different-phase faults, the establishment of universal voltage vectors enables fault-tolerant operation without the need for readjustment based on the fault phase location, which exhibit excellent fault tolerance performance and universality.

The rest of this article is organized as follows. Section II illustrates the open-switch fault analysis and universal fault-tolerant idea. In Section III, the simplified open-switch fault diagnosis is introduced, including fault characteristic and fault diagnosis criteria. Section IV provides a comprehensive introduction of postfault voltage vectors. Furthermore, the universal fault-tolerant SVPWM method is exhibited in Section V. Experimental results are presented in Section VI. Finally, Section VII concludes this article.

II. Open-Switch Fault Analysis and Universal Fault-Tolerant Idea

A. Open-Switch Fault Analysis

The open-circuit fault is common in electric drive systems and may appear in any module location. Fig. 1 illustrates the five-phase PMSM drive system. Subsequently, open circuit fault will predominantly manifest in the power devices of the inverter, motor windings, and connecting lines.

Usually, the damage of one motor winding or connecting line will results in the loss of an entire phase in motor system, which can also be referred to single open-phase fault. In the inverter, each phase contains two switch tubes. If both switch tubes on the same phase experience open-circuit fault simultaneously, this condition can also be classified as single open-phase fault.

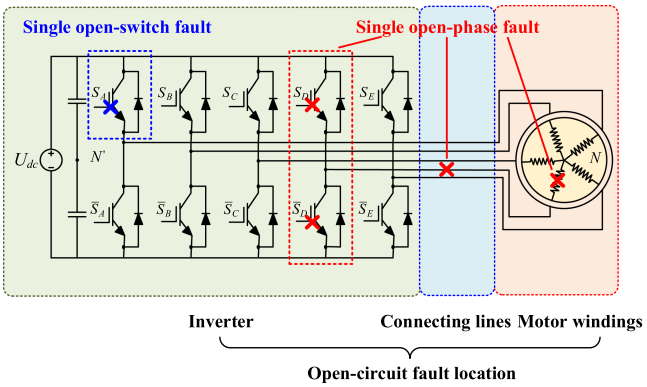

Fig. 1. Five-phase PMSM drive system with open-circuit fault location.

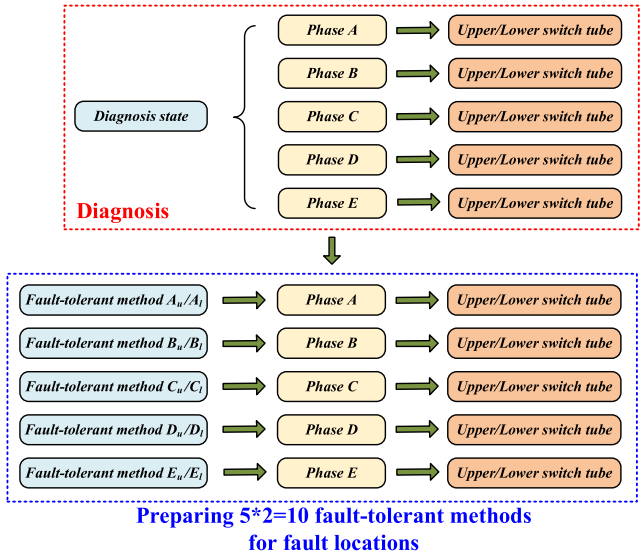

Fig. 2. Flowchart of traditional fault-tolerant method and fault diagnosis.

Conversely, if only one switch tube on a phase experience open-circuit fault while the other remains healthy, it is categorized as single open-switch fault.

Although there are numerous fault tolerant methods for single open-phase fault, directly applying these methods to single open-switch fault is equivalent to cutting two switch tubes in one phase from drive system. This fails to fully utilize the other healthy switch tube in the same phase, leading to low power device utilization rate and increasing the load on the power devices of the remaining phases. Hence, it is significant to treat single open-switch fault as a novel type of open-circuit fault and effectively utilize the healthy switch tube in faulty phase instead of directly applying conventional open-phase fault-tolerant methods.

B. Universal Fault-Tolerant Idea

On the other hand, common fault-tolerant strategies necessitate reconfiguration based on specific fault locations. Fig. 2 illustrates the flowchart of traditional fault-tolerant method and fault diagnosis. To make an assumption, the designed fault-tolerant

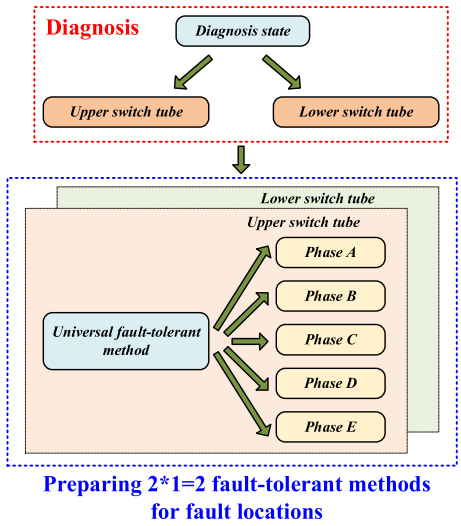

Fig. 3. Idea of universal fault-tolerant method with simplified fault diagnosis.

method is suitable for phase A fault. When fault occurs in phase B, this method cannot be directly applied without modification. Consequently, as the fault location changes, the core variables and parameters of the original fault-tolerant method A must also be adjusted accordingly. The fault-tolerant method A is switched to fault-tolerant method B. For five-phase PMSM, it requires to prepare five fault-tolerant methods to address faults in different phases. Additionally, since each-phase open-switch fault can occur in either the upper or lower switch tube, a total of ten fault-tolerant methods need to be prepared to comprehensively cover all possible fault scenarios. Simultaneously, the corresponding open-switch fault diagnosis must also distinguish ten different fault states in different phases, which makes the diagnosis process considerably more complex.

To achieve the principles of universality and simplification, it is crucial to consider the capability of adapting to phase changes without necessitating precise identification of the fault phase. Hence, it requires to design the universal fault tolerant method to deal with different-phase fault locations uniformly.

Single open-switch fault can occur in upper switch tube or the lower switch tube. If only one method is designed to handle all 10 single open-switch faults uniformly, it will inevitably encompass the unification of upper and lower switch tube faults. However, the unification of upper and lower switch tube faults will make the handling of open-switch fault revert to the handling method for open-phase fault. This leads to the loss of the single open-switch fault's distinct characteristic and does not fully utilize the other healthy switch tube within the same phase. And the unification process will also be very complicated.

Hence, it is advisable to prepare two universal fault-tolerant methods. The corresponding idea of universal fault-tolerant method with simplified fault diagnosis is illustrated in Fig. 3. The two methods, respectively, address five different-phase upper tube faults or lower tube faults. Compared with traditional approaches that require preparation of ten separate methods, this strategy significantly reduces the cost associated with algorithm

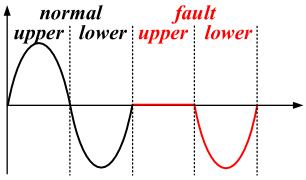

Fig. 4. Phase A current waveform under normal and fault conditions.

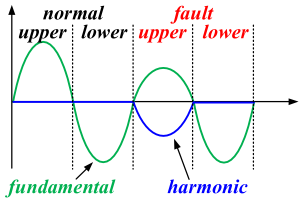

Fig. 5. Fundamental and harmonic components of phase A current.

switching. After the universal fault-tolerant method is realized, only an overall diagnosis to determine whether inverter involves an upper or lower tube fault is required to match the universal fault-tolerant algorithm, thereby simplifying the diagnosis process. The following sections will provide detailed information of simplified diagnosis procedures and universal fault-tolerant strategy.

III. Simplified Open-Switch Fault Diagnosis

A. Characteristic of Open-Switch Fault

When open-switch fault occurs, the phase current can be divided into the upper half cycle and the lower half cycle within one electrical cycle. Suppose open-switch fault occurs in phase A upper tube, the phase A current can be expressed as a combination within healthy and faulty half cycle

$$i_{A\text{total}}^{\text{Fault}} = \begin{cases} 0 & \theta_e \in (0,\pi) \\ M\sin\theta_e < 0 & \theta_e \in (\pi, 2\pi) \end{cases} \tag{1}$$

where, $i_{A\text{total}}^{\text{Fault}}$ is the phase A current in one electrical cycle; θ_e is the electrical angle; M is the amplitude of phase current. The corresponding phase A current waveform under normal and fault conditions are shown in Fig. 4.

Generally, the phase current of the five-phase motor can be decomposed into its fundamental component and third harmonic component. Fig. 5 depicts the fundamental and harmonic components of phase current in Fig. 4, which is obtained and concluded from simulation and experiment results.

It is evident from Fig. 5 that the third harmonic component remains at 0 under normal conditions, while it exhibits a significant change when fault occurs. The distinct and easily identifiable characteristic can serve as a reliable basis for fault diagnosis. The further analysis is tried and provided below.

As shown in Fig. 6, the third harmonic components can be extracted from the phase current by using Clarke matrix and its inverse transformation.

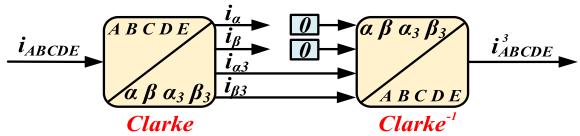

Fig. 6. Extraction of the third harmonic components.

The Clarke matrix and its inverse transformation are expressed as

$$T_{\text{clarke}} = \frac{2}{5}\begin{bmatrix} 1 & \cos\alpha & \cos 2\alpha & \cos 3\alpha & \cos 4\alpha \\ 0 & \sin\alpha & \sin 2\alpha & \sin 3\alpha & \sin 4\alpha \\ 1 & \cos 3\alpha & \cos 6\alpha & \cos 9\alpha & \cos 12\alpha \\ 0 & \sin 3\alpha & \sin 6\alpha & \sin 9\alpha & \sin 12\alpha \\ \sqrt{1/2} & \sqrt{1/2} & \sqrt{1/2} & \sqrt{1/2} & \sqrt{1/2} \end{bmatrix}$$
$$= \begin{bmatrix} 0.4 & 0.1236 & -0.3236 & -0.3236 & 0.1236 \\ 0 & 0.3804 & 0.2351 & -0.2351 & -0.3804 \\ 0.4 & -0.3236 & 0.1236 & 0.1236 & -0.3236 \\ 0 & -0.2351 & 0.3804 & -0.3804 & 0.2351 \\ 0.2828 & 0.2828 & 0.2828 & 0.2828 & 0.2828 \end{bmatrix} \tag{2}$$

$$T_{\text{Clarke}}^{-1} = \begin{bmatrix} 1 & 0 & 1 & 0 & \sqrt{1/2} \\ \cos\alpha & \sin\alpha & \cos 3\alpha & \sin 3\alpha & \sqrt{1/2} \\ \cos 2\alpha & \sin 2\alpha & \cos 6\alpha & \sin 6\alpha & \sqrt{1/2} \\ \cos 3\alpha & \sin 3\alpha & \cos 9\alpha & \sin 9\alpha & \sqrt{1/2} \\ \cos 4\alpha & \sin 4\alpha & \cos 12\alpha & \sin 12\alpha & \sqrt{1/2} \end{bmatrix}$$
$$= \begin{bmatrix} 1 & 0 & 1 & 0 & 0.7071 \\ 0.309 & 0.9511 & -0.809 & -0.5878 & 0.7071 \\ -0.809 & 0.5878 & 0.309 & 0.9511 & 0.7071 \\ -0.809 & -0.5878 & 0.309 & -0.9511 & 0.7071 \\ 0.309 & -0.9511 & -0.809 & 0.5878 & 0.7071 \end{bmatrix} \tag{3}$$

where, $\alpha = 2/5\pi$. Because the third harmonic subspace of the five-phase motor does not participate in the electromechanical energy conversion, the current of the tertiary space remains 0 under normal operation. Through the third and fourth rows of Clarke matrix (2), the α_3-axis and β_3-axis current can be transformed from five-phase currents

$$\begin{cases} i_{\alpha 3} = 0.4\,(i_A - 0.809 i_B + 0.309 i_C + 0.309 i_D - 0.809 i_E) = 0 \\ i_{\beta 3} = 0.4\,(-0.5878 i_B + 0.9511 i_C - 0.9511 i_D + 0.5878 i_E) = 0 \end{cases} \tag{4}$$

where i_x (x = A B C D E) is five-phase current under normal condition; $i_{\alpha 3}$ and $i_{\beta 3}$ are α_3-axis and β_3-axis current.

Through the inverse transformation of the Clarke matrix (3), the third harmonic component of the phase current can be obtained as

$$\begin{cases} i_{A3} = 0.4\,(-0.809 i_B + 0.309 i_C + 0.309 i_D - 0.809 i_E + i_A) = 0 \\ i_{B3} = 0.4(-0.809 i_A - 0.809 i_C + 0.309 i_D + 0.309 i_E + i_B) = 0 \\ i_{C3} = 0.4\,(0.309 i_A - 0.809 i_B - 0.809 i_D + 0.309 i_E + i_C) = 0 \\ i_{D3} = 0.4\,(0.309 i_A + 0.309 i_B - 0.809 i_C - 0.809 i_E + i_D) = 0 \\ i_{E3} = 0.4(-0.809 i_A + 0.309 i_B + 0.309 i_C - 0.809 i_D + i_E) = 0. \end{cases} \tag{5}$$

Using (5) as a benchmark, any postfault subtle deviation can serve as a diagnostic indicator. When phase A upper tube fault occurs, the absence of phase A current (iFault $A = 0$) disrupts the system balance, resulting in nonzero harmonic currents in each phase within faulty upper half cycle. The third harmonic component after fault can be adjusted as

$$\begin{cases} i_{A3}^{\text{Fault}} = 0.4\begin{pmatrix} -0.809i_B^{\text{Fault}} + 0.309i_C^{\text{Fault}} + 0.309i_D^{\text{Fault}} \\ -0.809i_E^{\text{Fault}} + i_A^{\text{Fault}}(0) \end{pmatrix} \\ i_{B3}^{\text{Fault}} = 0.4\begin{pmatrix} -0.809i_A^{\text{Fault}}(0) - 0.809i_C^{\text{Fault}} + 0.309i_D^{\text{Fault}} \\ +0.309i_E^{\text{Fault}} + i_B^{\text{Fault}} \end{pmatrix} \\ i_{C3}^{\text{Fault}} = 0.4\begin{pmatrix} 0.309i_A^{\text{Fault}}(0) - 0.809i_B^{\text{Fault}} - 0.809i_D^{\text{Fault}} \\ +0.309i_E^{\text{Fault}} + i_C^{\text{Fault}} \end{pmatrix} \\ i_{D3}^{\text{Fault}} = 0.4\begin{pmatrix} 0.309i_A^{\text{Fault}}(0) + 0.309i_B^{\text{Fault}} - 0.809i_C^{\text{Fault}} \\ -0.809i_E^{\text{Fault}} + i_D^{\text{Fault}} \end{pmatrix} \\ i_{E3}^{\text{Fault}} = 0.4\begin{pmatrix} -0.809i_A^{\text{Fault}}(0) + 0.309i_B^{\text{Fault}} + 0.309i_C^{\text{Fault}} \\ -0.809i_D^{\text{Fault}} + i_E^{\text{Fault}} \end{pmatrix} \end{cases} \tag{6}$$

where, i_x^{Fault} ($x = A\ B\ C\ D\ E$) is five-phase current after fault occurrence; i_{x3} ($x = A\ B\ C\ D\ E$) is the third harmonic component of phase current under normal operation; i_{x3}^{Fault} ($x = A\ B\ C\ D\ E$) is the third harmonic component of phase current after fault occurrence.

Simultaneously, whether under normal or single open-switch fault conditions, the phase currents must conform to the principle that the sum of the neutral point currents equals zero. Hence, the third harmonic component of phase current after fault occurrence should also satisfy the following condition:

$$i_{A3}^{\text{Fault}} + i_{B3}^{\text{Fault}} + i_{C3}^{\text{Fault}} + i_{D3}^{\text{Fault}} + i_{E3}^{\text{Fault}} = 0. \tag{7}$$

It is worth noting that the objective of diagnosis is to determine whether the fault lies in the upper tube or the lower tube in whole inverter. Therefore, it does not require to determine the exact value of the harmonic current in order to accurately identify the fault location of the faulty switch tube on a particular phase. It is only necessary to distinguish among the three states: the overall upper tube fault of the inverter, the overall lower tube fault of the inverter, or the normal state. More emphasis is placed on its positive and negative polarity relationship.

The probability that the third harmonic current within fault half cycle remains at 0 is extremely nonexistent. Hence, by comparing the constant zero value of the third harmonic current under normal conditions with the nonzero value that appears under single open-switch fault, the differentiation between normal and fault states can be achieved Then, the next step is to investigate the distinctions between upper switch tube fault and lower switch tube fault.

Since the third harmonic components of five-phase currents after fault can be either positive or negative, there must be [N] positive values and [5-N] negative values. Because, the upper switch tube fault and lower switch tube fault of the inverter exhibits an inverse relationship, meaning the number of their positive and negative values should be opposite. Suppose fault occurs in phase A upper switch tube, phase A current within upper halt cycle changes from $i_A > 0$ to 0. At this time, the third harmonic components of five-phase currents contains [x] positive values and [y] negative values. Conversely, when fault occurs in phase A lower switch tube, phase A current within upper halt cycle changes from $i_A < 0$ to 0. Correspondingly, the third harmonic components of five-phase currents will then exhibit [y] positive cycles and [x] negative cycles. For the correctness of this analysis, the positive and negative polarity relationship will be validated through simulation in Section VI-B, and further experimental verification will be conducted in Section VI.

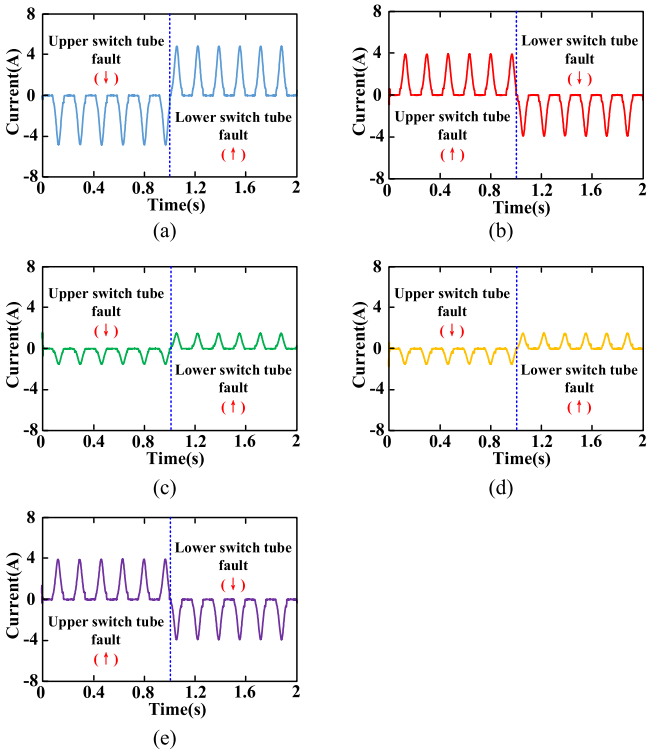

Fig. 7. Third harmonic components of five-phase currents (200 r/min). (a) Phase A. (b) Phase B. (c) Phase C. (d) Phase D. (e) Phase E.

B. Fault Diagnosis Criteria

Based on the analysis of the third harmonic part of the phase current in Section III-A, the corresponding Simulink simulation model is built to verify the feasibility.

In the simulation model, the five-phase motor operates for 2 s and the load is 5 Nm. To enhance persuasiveness, two groups of simulation results are simulated at the speed of 200 r/min and 400 r/min,, respectively. The initial state is to simulate phase A upper switch tube fault, and the state is changed to phase A lower switch tube fault one second later. As illustrated in Figs. 7 and 8, regardless of whether the fault occurs in the upper or lower switch tube, the third harmonic current waveform can be characterized as a combination of a "0 value" in healthy half cycle and a "positive or negative value" in faulty half cycle. During their own faulty half cycle, the upper switch tube fault exhibits 2 positive values and 3 negative values, whereas the lower switch tube fault displays 3 positive values and 2 negative values. The simulation result aligns with the analysis conducted in Section III-A.

The following is a simple analysis of this simulation result. The relationship of the third harmonic currents in (6) can be transformed as (8) shown at the bottom of this page, where, Δi_x ($x = B\ C\ D\ E$) is the main variation in the amplitude of phase current from normal to faulty condition.

Combining (8) with the relationship between i_B, i_C, i_D, i_E, and i_A in (5), the third harmonic component can be further simplified as

$$\begin{cases} i_{A3}^{Fault} = 0.4(-i_A) + 0.4\begin{pmatrix} -0.809_{\Delta}i_B + 0.309_{\Delta}i_C \\ +0.309_{\Delta}i_D + 0.809_{\Delta}i_E \end{pmatrix} \\ i_{B3}^{Fault} = 0.4(0.809i_A) + 0.4\begin{pmatrix} -0.809_{\Delta}i_C + 0.309_{\Delta}i_D \\ +0.309_{\Delta}i_E + {}_{\Delta}i_B \end{pmatrix} \\ i_{C3}^{Fault} = 0.4(-0.309i_A) + 0.4\begin{pmatrix} -0.809_{\Delta}i_B - 0.809_{\Delta}i_D \\ +0.309_{\Delta}i_E + {}_{\Delta}i_C \end{pmatrix} \\ i_{D3}^{Fault} = 0.4(-0.309i_A) + 0.4\begin{pmatrix} 0.309_{\Delta}i_B - 0.809_{\Delta}i_C \\ -0.809_{\Delta}i_E + {}_{\Delta}i_D \end{pmatrix} \\ i_{E3}^{Fault} = 0.4(0.809i_A) + 0.4\begin{pmatrix} 0.309_{\Delta}i_B + 0.309_{\Delta}i_C \\ -0.809_{\Delta}i_D + {}_{\Delta}i_E \end{pmatrix} \end{cases} \tag{9}$$

It can be seen from the simulation results in Figs. 7 and 8 that the positive and negative relationship of the five-phase third harmonic current during faulty half cycle is mainly determined by the former components 0.4(-i_A), 0.4(0.809i_A), 0.4(-0.309i_A), 0.4(-0.309i_A), 0.4(0.809i_A) in (9). According to the experimental results of existed [20], [21], [22] and this article, the amplitude variation of the remaining healthy phase current under single open-switch fault can be evaluated as relatively small compared with the original phase current amplitude. Hence, the latter components of (9) has minor influence in the positive and negative relationship. Its influence is insufficient to alter the judgment of positive and negative values. Therefore, it is disregarded in this article. Even if it overturns the original positive and negative values, the number of positive and negative values on upper switch tube fault changes from [x y] to [x+Δ y-Δ]. Due to the existence of inverse relationship, the number of positive and negative values on lower switch tube fault will also be transformed to [y-Δ x+Δ]. As long as the characteristics of upper switch fault and the lower switch fault are opposite to each other, it will not affect the distinction between the two types of faults.

Subsequently, the third harmonic current exhibits a state that is greater than or equal to 0 (↑) or less than or equal to 0 (↓), which can serve as a diagnostic indicator. In case of phase A upper tube fault, the third harmonic component exhibits 3 (↓) and 2 (↑); whereas, in case of phase A lower tube fault, it manifests 2 (↓) and 3 (↑). Due to the symmetrical structure of the five-phase motor, the numbers of (↓) and (↑) under upper or lower switch tube faults in the other phases are identical. Since phase A upper tube fault contains 3 (↓) and 2 (↑), then phase B, C, D, and E upper tube fault will also exhibit the same numbers of 3 (↓) and 2 (↑). Only the phase location of positive and negative values will be changed, but the total numbers of positive and negative values remain the same.

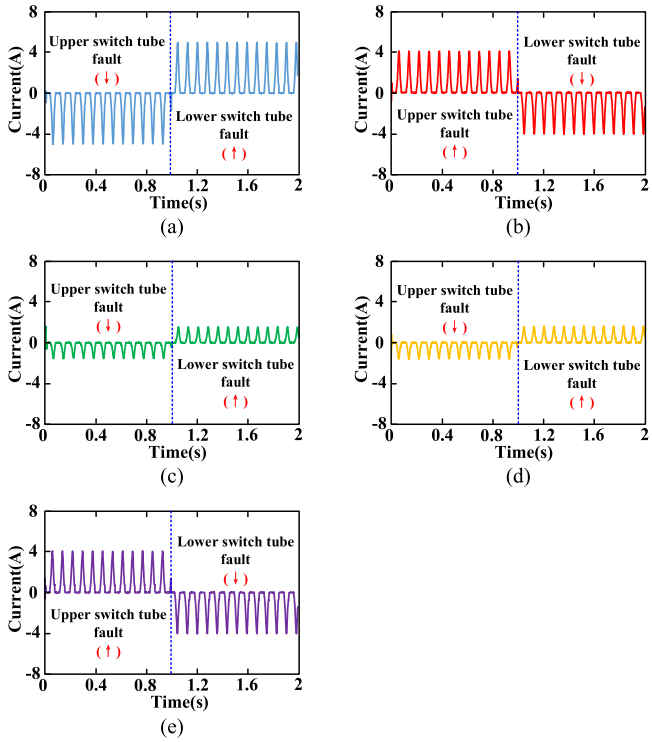

Fig. 8. Third harmonic components of five-phase currents (400 r/min). (a) Phase A. (b) Phase B. (c) Phase C. (d) Phase D. (e) Phase E.

In conclusion, the characteristics of upper and lower switch tube faults are entirely opposite, making them easily distinguishable and reducing the likelihood of misdiagnosis. The whole simplified open-switch fault diagnosis flowchart is depicted in Fig. 9.

To count the positive and negative values in practical application, the average values of third harmonic currents can be

$$\begin{cases} i_{A3}^{Fault} = 0.4\begin{pmatrix} -0.809(i_B + {}_{\Delta}i_B) + 0.309(i_C + {}_{\Delta}i_C) + 0.309(i_D + {}_{\Delta}i_D) \\ -0.809(i_E + {}_{\Delta}i_E) + (i_A - i_A) \end{pmatrix} \\ i_{B3}^{Fault} = 0.4\begin{pmatrix} -0.809(i_A - i_A) - 0.809(i_C + {}_{\Delta}i_C) + 0.309(i_D + {}_{\Delta}i_D) \\ +0.309(i_E + {}_{\Delta}i_E) + (i_B + {}_{\Delta}i_B) \end{pmatrix} \\ i_{C3}^{Fault} = 0.4\begin{pmatrix} 0.309(i_A - i_A) - 0.809(i_B + {}_{\Delta}i_B) - 0.809(i_D + {}_{\Delta}i_D) \\ +0.309(i_E + {}_{\Delta}i_E) + (i_C + {}_{\Delta}i_C) \end{pmatrix} \\ i_{D3}^{Fault} = 0.4\begin{pmatrix} 0.309(i_A - i_A) + 0.309(i_B + {}_{\Delta}i_B) - 0.809(i_C + {}_{\Delta}i_C) \\ -0.809(i_E + {}_{\Delta}i_E) + (i_D + {}_{\Delta}i_D) \end{pmatrix} \\ i_{E3}^{Fault} = 0.4\begin{pmatrix} -0.809(i_A - i_A) + 0.309(i_B + {}_{\Delta}i_B) + 0.309(i_C + {}_{\Delta}i_C) \\ -0.809(i_D + {}_{\Delta}i_D) + (i_E + {}_{\Delta}i_E) \end{pmatrix} \end{cases} \tag{8}$$

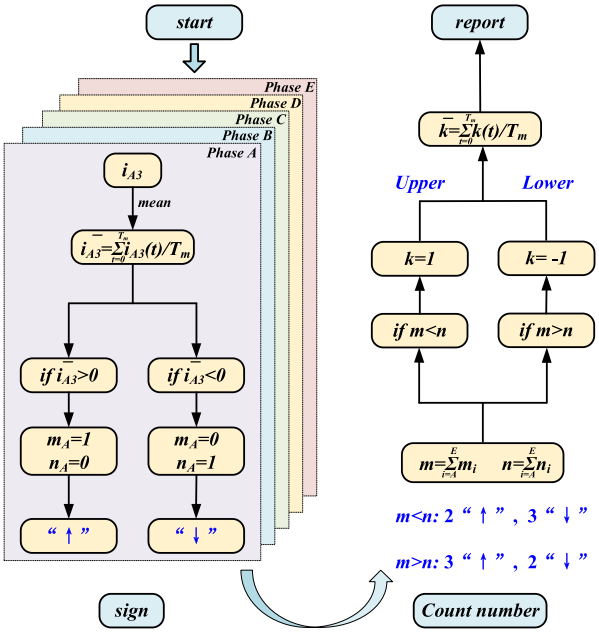

Fig. 9. Simplified open-switch fault diagnosis flowchart.

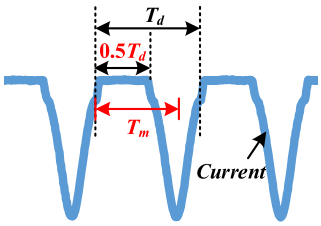

Fig. 10. Setting of the specific time period.

calculated over a specific time period, which are illustrated as

$$\overline{i_{A3}} = \sum_{t=0}^{T_m} i_A(t)/T_m, T_m > 0.5T_d = \frac{30}{n_e p} \tag{10}$$

where p is the pole pairs; n_e is the motor speed; T_{d} is the electrical cycle; T_{m} is the specific time period, as shown in Fig. 10. Theoretically, when T_{m} exceeds 0.5 electrical cycle (T_{d}), the diagnosis algorithm can be achieved. Furthermore, the diagnosis time mainly depends on the value of T_m.

When the average value exceeds zero, it signifies a positive fluctuation; conversely, when the average value is below zero, it denotes a negative fluctuation. In the flowchart, m and n, respectively, record the number of positive and negative values; while, k is a sign of diagnosis to compare m with n. When k equals 1, the upper tube is deemed faulty; whereas when k equals -1, the lower tube is considered faulty. To eliminate any accidental errors, the average value of k is calculated at the end. Simultaneously, this ensures that k represents the median value while fluctuating around 0 in a nonfault state for the motor.

In general, the diagnosis algorithm is fundamentally based on the characteristics of the third harmonic current when the upper or lower switch tube are faulty. Consequently, it does not incorporate actual motor parameters such as resistance, inductance, and flux linkage. Additionally, m, n, and k serve as storage variables for system calculations, which basically remain unchanged. While, the setting of T_m is automatically adjusted according to real-time speed changes. The accuracy of T_m primarily depends on the precision of the position sensor and generally do not result in significant fluctuations. Therefore, the accuracy of this diagnosis method is minimally affected by parameter variations.

TABLE I
HEALTHY AND FAULTY VOLTAGE EXCITATIONS OF INFLUENCED SWITCHING STATES

States	Healthy (U_{dc})					Faulty (U_{dc})				
	U_{AN}	U_{BN}	U_{CN}	U_{DN}	U_{EN}	U_{AN}	U_{BN}	U_{CN}	U_{DN}	U_{EN}
10000	4/5	-1/5	-1/5	-1/5	-1/5	0	0	0	0	0
10001	3/5	-2/5	-2/5	-2/5	3/5	0	-1/4	-1/4	-1/4	3/4
10010	3/5	-2/5	-2/5	3/5	-2/5	0	-1/4	-1/4	3/4	-1/4
10011	2/5	-3/5	-3/5	2/5	2/5	0	-1/2	-1/2	1/2	1/2
10100	3/5	-2/5	3/5	-2/5	-2/5	0	-1/4	3/4	-1/4	-1/4
10101	2/5	-3/5	2/5	-3/5	2/5	0	-1/2	1/2	-1/2	1/2
10110	2/5	-3/5	2/5	2/5	-3/5	0	-1/2	1/2	1/2	-1/2
10111	1/5	-4/5	1/5	1/5	1/5	0	-3/4	1/4	1/4	1/4
11000	3/5	3/5	-2/5	-2/5	-2/5	0	3/4	-1/4	-1/4	-1/4
11001	2/5	2/5	-3/5	-3/5	2/5	0	1/2	-1/2	-1/2	1/2
11010	2/5	2/5	-3/5	2/5	-3/5	0	1/2	-1/2	1/2	-1/2
11011	1/5	1/5	-4/5	1/5	1/5	0	1/4	-3/4	1/4	1/4
11100	2/5	2/5	2/5	-3/5	-3/5	0	1/2	1/2	-1/2	-1/2
11101	1/5	1/5	1/5	-4/5	1/5	0	1/4	1/4	-3/4	1/4
11110	1/5	1/5	1/5	1/5	-4/5	0	1/4	1/4	1/4	-3/4
11111	0	0	0	0	0	0	0	0	0	0

IV. POSTFAULT VOLTAGE VECTORS

At the beginning of designing a universal fault-tolerant strategy, it is essential to analyze the changes of inverter voltage vectors caused by open-switch fault. This section takes phase A upper switch tube fault as an example to introduce the vector reconstruction and synthesis after the fault. Then, the characteristics of various phase open-switch faults are systematically summarized in Section V.

A. Reconstruction of Inverter Space Voltage Vectors

The five-phase two-level voltage source inverter can generate $2^5 = 32$ switching states. In each phase of the inverter, "1" indicates upper leg is open while "0" indicates the opposite. In case of single open-switch fault, the intended bridge arm passage will be closed, which results in an impact on $2^4 = 16$ related voltage vectors.

Taking phase A upper tube fault as an example, the phase voltage excitations of the "1$xxxx$ (x = 0&1)" switching state will be changed. Correspondingly, the affected voltage vectors include U_{16}–U_{31}. The healthy and faulty voltage excitations of the influenced switching states are summarized in Table I.

On the basis of the voltage excitations of each switching state, the faulty voltage vectors in α-β frame and α_3-β_3 frame can be deduced by

$$\begin{cases} U_{\alpha\beta} = \frac{2}{5}\left(U_{AN} + U_{BN}e^{j\alpha} + U_{CN}e^{j2\alpha} + U_{DN}e^{j3\alpha} \right. \\ \qquad \left. + U_{EN}e^{j4\alpha}\right) \\ U_{\alpha\beta 3} = \frac{2}{5}\left(U_{AN} + U_{CN}e^{j\alpha} + U_{EN}e^{j2\alpha} + U_{BN}e^{j3\alpha} \right. \\ \qquad \left. + U_{DN}e^{j4\alpha}\right) \end{cases} \tag{11}$$

TABLE II
AMPLITUDES AND DIRECTIONS OF INFLUENCED VOLTAGE VECTORS

Influenced vectors: U_{16}–U_{31} (Null vectors: U_{16} and U_{31})							
Vector	U_{17}	U_{18}	U_{19}	U_{20}	U_{21}	U_{22}	U_{23}
$\lvert U_{\alpha\beta}\rvert(U_{dc})$	0.4413	0.3245	0.6155	0.3245	0.1453	0.4472	0.4413
$\theta_{\alpha\beta}(°)$	-59.6	-133.6	-90	133.6	-90	180	-120.4
$\lvert U_{\alpha\beta3}\rvert(U_{dc})$	0.3245	0.4413	0.1453	0.4413	0.6155	0.4472	0.3245
$\theta_{\alpha\beta3}(°)$	133.6	-59.6	-90	59.6	90	0	46.4
Vector	U_{24}	U_{25}	U_{26}	U_{27}	U_{28}	U_{29}	U_{30}
$\lvert U_{\alpha\beta}\rvert(U_{dc})$	0.4413	0.4472	0.1453	0.3245	0.6155	0.3245	0.4413
$\theta_{\alpha\beta}(°)$	59.6	0	90	-46.4	90	46.4	120.4
$\lvert U_{\alpha\beta3}\rvert(U_{dc})$	0.3245	0.4472	0.6155	0.4413	0.1453	0.4413	0.3245
$\theta_{\alpha\beta3}(°)$	-133.6	180	-90	-120.4	90	120.4	-46.4

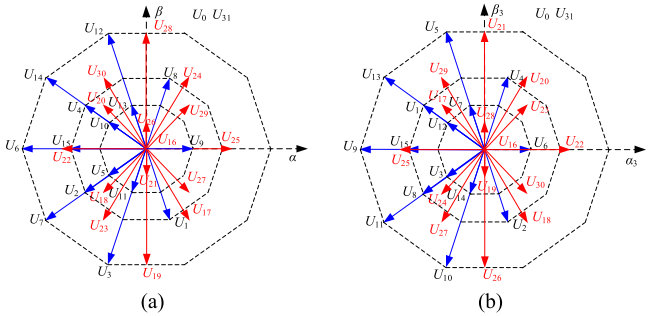

Fig. 11. Distribution of all basic voltage vectors under phase A upper switch tube fault. (a) α-β frame. (b) α_3-β_3 frame.

where $\alpha = 2/5\pi$; $U_{\rm dc}$ is dc bus voltage; $U_{\alpha\beta}$ is the voltage in α-β frame; $U_{\alpha\beta3}$ is the voltage in α_3-β_3 frame; U_{xN} (x = A, B, C, D, E) is the voltage excitation of each phase.

Substituting the voltage excitations under faulty condition in Table I into (11), the influenced voltage vectors can be concluded as Table II. Combined with the remaining unaffected vectors, the distribution of all basic voltage vectors under open-switch fault is depicted in Fig. 11. In comparison to voltage vectors under normal operation, voltage vectors under open-switch fault exhibit attenuation and deviation in amplitude and angle. It is precisely due to attenuation and deviation in voltage vectors that causes errors in the inverter output signal to the motor. This, in turn, affects the current closed-loop control in motor system and ultimately impacts output torque of the motor. The red lines represent vectors affected by fault (U_{16}–U_{31}), and the blue vectors are unaffected ones (U_0–U_{15}). Among unaffected voltage vectors, U_{12}, U_{14}, U_6, U_7, U_3 are still large voltages vectors ($0.6472U_{\rm dc}$) under normal condition; U_8, U_4, U_{15}, U_2, U_1 are still medium voltages vectors ($0.4U_{\rm dc}$) under normal condition; U_{13}, U_{10}, U_5, U_{11}, U_9 are still small voltages vectors ($0.2472U_{\rm dc}$) under normal condition.

Fig. 12 compares the modulation areas in α-β frame under single open-switch fault with that under single open-phase fault. As shown in Fig. 12(a), the modulation area is composed of ten large vectors, including affected ones and unaffected ones. While, the deficient modulation area is located on the right side of the spatial plane. This is because the affected large vectors are distributed in the right half of the space plane, resulting in loss of vector amplitude and reduction in the modulation area. If single open-switch fault is treated as single open phase fault, both U_{16}–U_{31} and U_0–U_{15} will be influenced. U_0–U_{15} will also

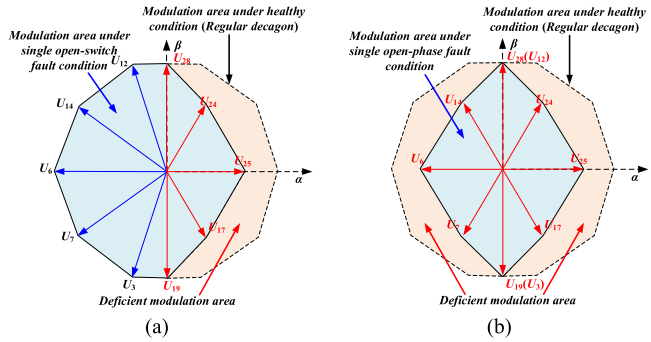

Fig. 12. Modulation areas in α-β frame under different faults. (a) Single open-switch fault (phase A upper switch tube fault). (b) Single open-phase fault (phase A).

be reconstructed according to the switching state analysis in Table I and the voltage equation in (11). Correspondingly, in Fig. 12(b), all ten large vectors are all influenced and exhibit symmetrical characteristics, highlighted in red lines. Compared with single open-switch fault, the deficient modulation area of single open-phase fault includes not only the right side but also the left side of the plane. The two deficient areas exhibit perfect symmetry. In other words, the existing open-phase fault-tolerant methods that involve vector changes will lack more extra modulation area compared with the proposed vector reconstruction for open-switch fault. This can be attributed to the proposed method's effective utilization of the other switch tube in faulty phase.

The modulation index of the fundamental subspace can be expressed as

$$M = \frac{|U_{ref}|}{0.5U_{\rm dc}}. \tag{12}$$

Under normal condition, the amplitude of the maximum linear voltage vector is the inscribed circle radius of regular decagon formed by large vectors. The maximum linear modulation index can be expressed as

$$M_{\rm linear} = \frac{0.6472U_{\rm dc} \times \cos(\pi/10)}{0.5U_{\rm dc}} = 1.231. \tag{13}$$

Under fault condition, vectors with varying amplitudes cannot form regular polygons. The maximum linear voltage vector is related to the minimum voltage vector. For the proposed vector reconstruction of open-switch fault, the maximum linear modulation index can be expressed as

$$M_{\rm linear} = \frac{0.4413U_{\rm dc}}{0.5U_{\rm dc}} = 0.8826. \tag{14}$$

For the existing vector-change fault-tolerant method in [17], which gives up the entire phase and constructs reduced-order matrix, the maximum linear modulation index can be expressed as

$$M_{\rm linear} = \frac{0.3804U_{\rm dc}}{0.5U_{\rm dc}} = 0.7608. \tag{15}$$

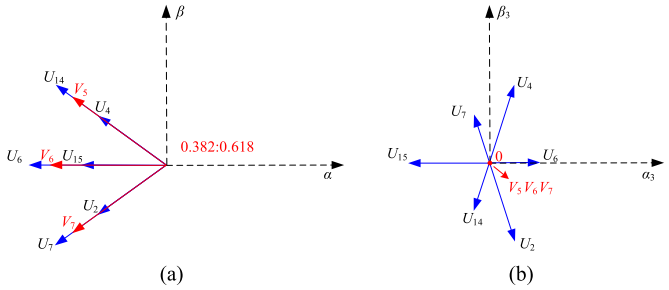

Fig. 13. Synthesis of unaffected voltage vectors under phase A upper switch tube fault. (a) α-β frame. (b) α_3-β_3 frame.

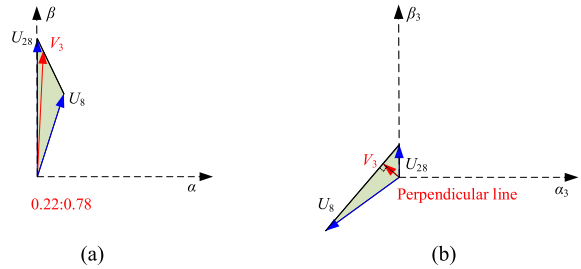

Fig. 14. Synthesis of affected voltage vectors under phase A upper switch tube fault (U_8 and U_{28}). (a) α-β frame. (b) α_3-β_3 frame.

Compared to the existing method that directly abandons the phase, the modulation index for the proposed vector reconstruction of open-switch fault is improved.

B. Synthesis of Virtual Voltage Vectors

The virtual voltage vectors are usually synthesized in SVPWM. Du et al. [15] introduced that the maximum linear modulation index for virtual voltage vector utilization under normal condition is expressed as

$$M_{\text{linear}} = \frac{0.5527U_{\text{dc}} \times \cos(\pi/10)}{0.5U_{\text{dc}}} = 1.0513. \tag{16}$$

Compared with (13) under normal condition, the modulation index is certainly reduced by 14.6%. However, the synthesis of virtual voltage vectors can reduce the influence of harmonic space and improve the control precision of SVPWM.

As depicted in Fig. 11, the vector distribution under fault condition is asymmetrical and complex. Hence, the voltage vectors need to be processed and simplified. Firstly, to reduce the scope of consideration, (U_5, U_9, U_{10}, U_{11}, U_{13}, U_{18}, U_{20}, U_{21}, U_{22}, U_{26}) with small amplitudes in the fundamental subspace are ignored. Then, the remaining vectors, which also correspond to large and medium vectors under normal condition can be organized into pairs as: [U_{16}, U_{25}], [U_{29}, U_{24}], [U_8, U_{28}], [U_{30}, U_{12}], [U_4, U_{14}], [U_{15}, U_6], [U_2, U_7], [U_{23}, U_3], [U_1, U_{19}], [U_{27}, U_{17}].

Type1. Unaffected Voltage Vectors: Among them, vectors [U_4, U_{14}], [U_{15}, U_6], [U_2, U_7] remain unaffected by open-switch fault. It can be seen from Fig. 13 that the two vectors of each combination are distributed in the same straight direction in two subspaces. Therefore, the action time ratio of 0.382:0.618 can be utilized to synthesize the voltage component in harmonic space as 0. Taking the fifth combination [U_4, U_{14}] as an example, the virtual voltage vector V_5 can be synthesized as

$$\begin{cases} \min\{\boldsymbol{V_{5\alpha\beta3}} = T_4\boldsymbol{U_{4\alpha\beta3}} + T_{14}\boldsymbol{U_{14\alpha\beta3}}\} = 0 \Rightarrow \frac{T_4}{T_{14}} = \frac{0.382}{0.618} \\ \boldsymbol{V_{5\alpha\beta}} = T_4\boldsymbol{U_{4\alpha\beta}} + T_{14}\boldsymbol{U_{14\alpha\beta}}, \boldsymbol{V_{5\alpha\beta3}} = 0 \end{cases} \tag{17}$$

where $\boldsymbol{U_{4\alpha\beta}}$, $\boldsymbol{U_{14\alpha\beta}}$, and $\boldsymbol{V_{5\alpha\beta}}$ are the voltage component of U_4, U_{14}, and V_5 in α-β frame, respectively; $\boldsymbol{U_{4\alpha\beta3}}$, $\boldsymbol{U_{14\alpha\beta3}}$, and $\boldsymbol{V_{5\alpha\beta3}}$ are the voltage component in α_3-β_3 frame, respectively; T_4 and T_{14} are the action U_4 and U_{14}.

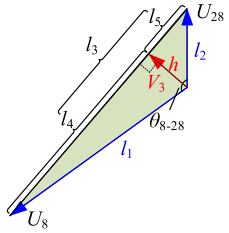

Fig. 15. Calculation of action time (U_8 and U_{28}).

Type2. Affected Voltage Vectors: For vectors affected by open-switch fault, the two vectors of each combination are distributed in different directions. In other words, the voltage component in harmonic space cannot be synthesized to 0 in the same straight line. At this time, the current criterion for resolving the action time shifts to minimizing the amplitude of the synthesized voltage vector in harmonic space.

Taking the third combination [U_8, U_{28}] as an example, it can be seen from Fig. 14 that the range of motion of the synthesized virtual voltage vector's vertex is the third edge of the triangle formed by the two vectors. The criterion of minimizing the amplitude of the synthesized voltage vector becomes a mathematical problem of finding the position closest to the origin on the third edge, which can be obtained by drawing a perpendicular line. Then, the action time can be solved by applying mathematical principles.

In Fig. 15, l_1 ($0.4U_{\text{dc}}$) and l_2 ($0.1453U_{\text{dc}}$) represent the length of U_8 and U_{28}; $\theta_{8\text{-}28}$ (126°) represents the angle between two vectors. In accordance with the law of cosines, the length of the third side l_3 and the altitude of a triangle h can be determined as

$$\begin{aligned} l_3 &= \sqrt{{l_1}^2 + {l_2}^2 - 2\cos\theta_{8-28} l_1 l_2} \\ h &= \frac{l_1 l_2 \sin\theta_{8-28}}{l_3}. \end{aligned} \tag{18}$$

Furthermore, l_4 and l_5 can be obtained as

$$l_4 = \sqrt{{l_1}^2 - h^2}, l_5 = \sqrt{{l_2}^2 - h^2}. \tag{19}$$

According to the principles of triangle theory, the ratio of l_5/l_4 is the action time ratio of [U_8, U_{28}]. Finally, the action time can be determined as 0.22:0.78 and the virtual voltage vector

TABLE III
ACTION TIME RATIOS AND LOCATIONS OF SYNTHESIZED VIRTUAL VOLTAGE VECTORS

Group		Action time ratio	$\lvert V_{\alpha\beta}\rvert(U_{dc})$	$\theta_{\alpha\beta}(°)$	$\lvert V_{\alpha\beta3}\rvert(U_{dc})$	$\theta_{\alpha\beta3}(°)$
V_1	$[U_{16}, U_{25}]$	0:1	0.4472	0	0.4472	180
V_2	$[U_{29}, U_{24}]$	0.383:0.617	0.3944	55.4	0.2236	179.9
V_3	$[U_8, U_{28}]$	0.22:0.78	0.5644	87.2	0.0941	139.1
V_4	$[U_{30}, U_{12}]$	0.43:0.57	0.5553	112.2	0.0255	228.3
V_5	$[U_4, U_{14}]$	0.382:0.618	0.5528	144	0	0
V_6	$[U_{15}, U_6]$	0.382:0.618	0.5528	180	0	0
V_7	$[U_2, U_7]$	0.382:0.618	0.5528	216	0	0
V_8	$[U_{23}, U_3]$	0.43:0.57	0.5553	247.8	0.0255	131.7
V_9	$[U_1, U_{19}]$	0.22:0.78	0.5644	272.8	0.0941	220.9
V_{10}	$[U_{27}, U_{17}]$	0.383:0.617	0.3944	304.6	0.2236	180.1

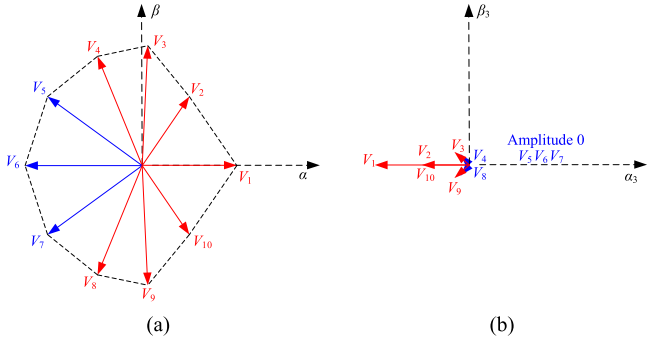

Fig. 16. Distribution of virtual voltage vectors under phase A upper switch tube fault. (a) α-β frame. (b) α_3-β_3 frame.

can be synthesized as

$$\begin{cases} \min\{\boldsymbol{V_{3\alpha\beta3}} = T_8\boldsymbol{U_{8\alpha\beta3}} + T_{28}\boldsymbol{U_{28\alpha\beta3}}\} \neq 0 \Rightarrow \frac{T_8}{T_{28}} = \frac{0.22}{0.78} \\ \boldsymbol{V_{3\alpha\beta}} = T_8\boldsymbol{U_{8\alpha\beta}} + T_{28}\boldsymbol{U_{28\alpha\beta}}, \boldsymbol{V_{3\alpha\beta3}} = T_8\boldsymbol{U_{8\alpha\beta3}} \\ \qquad\qquad + T_{28}\boldsymbol{U_{28\alpha\beta3}} \end{cases} \tag{20}$$

where $\boldsymbol{U_{8\alpha\beta}}$, $\boldsymbol{U_{28\alpha\beta}}$, and $\boldsymbol{V_{3\alpha\beta}}$ are the voltage component of U_8, U_{28}, and V_3 in α-β frame, respectively; $\boldsymbol{U_{8\alpha\beta3}}$, $\boldsymbol{U_{28\alpha\beta3}}$, and $\boldsymbol{V_{3\alpha\beta3}}$ are the voltage component in α3-β3 frame, respectively; T_8 and T_{28} are the action U_8 and U_{28}.

Similarly, the action time ratio of the other voltage vector combinations can be obtained. In particular, U_{16} is a newly generated null vector due to open-switch fault. Consequently, action time ratio of $[U_{16}, U_{25}]$ can be directly obtained as 0:1. Through synthesizing two vectors of each combination proportionally to their respective action time ratio, the virtual voltage vectors under open-switch fault can be obtained, which are defined as V_1–V_{10}. The amplitudes and directions of synthesized virtual voltage vectors are concluded in Table III and their distribution is depicted in Fig. 16.

Compared with Fig. 11, the amplitude of voltage vectors inharmonic space is significantly reduced. Meanwhile, the maximum linear modulation index for virtual voltage vector utilization under single open-switch fault can be expressed as

$$M_{\text{linear}} = \frac{0.3944U_{\text{dc}}}{0.5U_{\text{dc}}} = 0.7888. \tag{21}$$

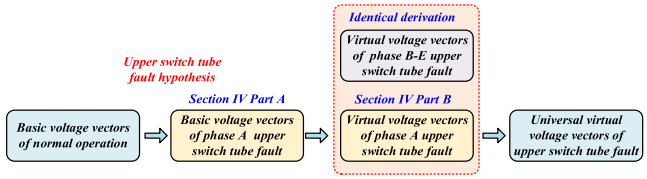

Fig. 17. Evolution process of universal virtual voltage vectors.

Compared with (14) before the synthesis of virtual voltage vectors, the modulation index is certainly reduced by 10.6%. But the harmonic components of voltage in α_3-β_3 frame has been effectively suppressed. Nevertheless, the modulation index for virtual voltage vector utilization under single open-switch fault remains slightly above (15) for the existing vector-change fault-tolerant method, which gives up the entire phase and constructs reduced-order matrix.

V. UNIVERSAL FAULT-TOLERANT SVPWM STRATEGY

As shown in Fig. 17, both the reconstructed basic voltage vectors and synthesized virtual voltage vectors in Section IV is only applicable for single open-switch fault in one phase.

In order to ensure the applicability of the newly derived virtual voltage vectors to other phase open-switch fault, it becomes imperative to design universal virtual voltage vectors. There are three main steps as follows and the detailed information is introduced in Sections V-A, V-B, and V-C of this section.

Step 1: Establishing vector sets of five phases.
Step 2: Dividing sectors.
Step 3: Finding intersection regions.

A. Establishing Vector Sets of Five Phases

Since the diagnosis method in Section II successfully differentiated between the upper and lower tubes, only five-phase upper tube faults are selected as examples for the construction of universal voltage vectors under upper switch tube fault. And the identical addressing method is also applied to lower switch tube fault.

By referring to the derivation procedure in Section IV-B, the virtual voltage vectors for the remaining four-phase upper tube fault can be reconstructed in a similar manner. The distribution of virtual voltage vectors in α-β frame under arbitrary upper switch tube fault is depicted in Fig. 18(a)–(e).

The pattern shape of each phase distribution map is rotated by an angle of 72° relative to the previous phase. To obtain universal virtual voltage vectors, the distributions under five different upper switch tube fault are superimposed together as Fig. 18(f). There are five colors, and each color corresponds to the reconstructed vectors under each phase upper switch tube fault. Furthermore, all virtual voltage vectors collectively constitute ten novel vector sets of V_1–V_{10}. Each vector set comprises vectors in five distinct colors.

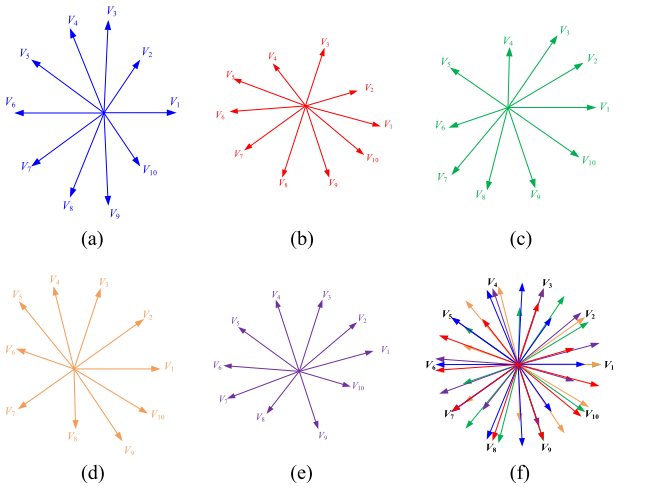

Fig. 18. Distribution of virtual voltage vectors under arbitrary upper switch tube fault. (a) Phase A. (b) Phase B. (c) Phase C. (d) Phase D. (e) Phase E. (f) Five-phase superposition.

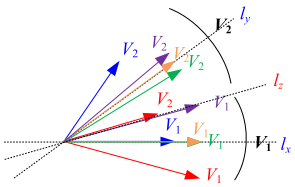

Fig. 19. Vector sets of V_1 and V_2.

B. Dividing Sectors

Since Fig. 18(f) contains all the virtual voltage vectors of five phases, the overall spatial plane exhibits very complex. To facilitate analysis, it is necessary to segment the sectors and subsequently proceed with the subsequent steps within each sector. Through observation, it can be found that the distribution of vector sets is regular. Taking V_1 and V_2 as examples, as illustrated in Fig. 19, their vector sets exhibit axisymmetric structures around l_x and l_y, respectively. In addition, the vector sets have closely adjacent boundaries, with a 16.5° angle for red V_2 and a 15.2° angle for purple V_1. Considering a straight line (l_z) at 16°, it precisely delineates the boundary between the two vector sets. Similarly, the remaining vector sets can also be partitioned by referring to l_x, l_y, and l_z.

As illustrated in Fig. 20, the entire plane can be divided into ten large sectors, ranging from I to X. Each large sector represents the range of each vector set. Moreover, the large sector can be further subdivided into two smaller sectors based on their symmetry properties, with each small sector being closely associated with the two vector sets that are closest to its own vector set. In total, there are 20 small sectors, ranging from 1 to 20. The angle ranges of large sectors and small sectors are concluded in Table IV.

C. Finding Intersection Regions

The next step is to determine intersection regions. This applies the barrel theory, which posits that the volume of water a barrel

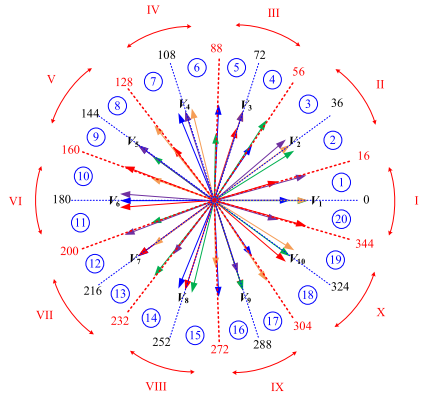

Fig. 20. Large sectors and small sectors.

TABLE IV
ANGLE RANGES OF LARGE SECTORS AND SMALL SECTORS

Large sectors	Small sectors	Angle range	Large sectors	Small sectors	Angle range
I	20	344–0	VI	10	160–180
	1	0–16		11	180–200
II	2	16–36	VII	12	200–216
	3	36–56		13	216–232
III	4	56–72	VIII	14	232–252
	5	72–88		15	252–272
IV	6	88–108	IX	16	272–288
	7	108–128		17	288–304
V	8	128–144	X	18	304–324
	9	144–160		19	324–344

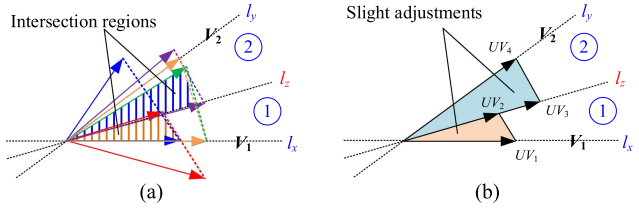

Fig. 21. Acquisition of universal modulation region of vector sets (V_1 and V_2). (a) Searching for the intersection of five regions. (b) Slight adjustments to the intersection.

can contain is determined not by the tallest stave but rather by the shortest one. Therefore, the universal fault tolerance method is also to obtain the maximum common area of reconstructed virtual voltage vectors under different-phase switching tube fault. As per usual practice, two vector sets (V_1 and V_2) are selected as illustrative examples. The modulation range of two virtual voltage vectors is typically a triangular region defined by these two vectors. In Fig. 21(a), five different kinds of V_1 and V_2 are, respectively, connected to obtain the corresponding modulation region. It can be found that the intersection of the five areas is primarily concentrated in two specific regions. The range of angle (0–31.8°) encompassed by these two regions (from the blue V_1 to the green V_2) closely approximate the range of angle (0–36°) for small sectors 1 and 2.

If the intersection area in Fig. 21(a) is directly utilized as the common area, it would fail to adequately encompass the full extent of sectors 1 and 2 (0–36°). In order to ensure entire coverage of all sectors and maintain continuous range of angle,

TABLE V
ACTION TIME RATIOS AND LOCATIONS OF UNIVERSAL VIRTUAL VOLTAGE VECTORS (SMALL SECTOR 1 AND 2)

Group		Action time ratio	Amplitudes (U_{dc})	Directions (°)
UV_1	[U_{16}, U_{25}]	0:1	0.4472	0
UV_2	[U_{29}, U_{24}]	0.383:0.617	0.3944	16
UV_3	[U_{16}, U_{25}]	0.22:0.78	0.5644	16
UV_4	[U_{29}, U_{24}]	0.382:0.618	0.5528	36

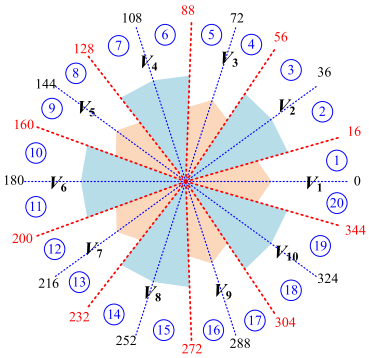

Fig. 22. Whole modulation region of all universal virtual voltage vectors.

the regions should be slightly adjusted. Therefore, adjust the upper boundary of the blue region in Fig. 21(a) to the yellow V_2, and define the lower boundary of the red region to the blue V_1. The boundaries of the junction region (specifically the lower boundary of the blue region and the upper boundary of the red region) still utilize purple V_2 and red V_1, respectively, with the angle uniformly set to 16°. As shown in Fig. 21(b), each small sector has two universal virtual voltage vectors (*UVs*) and there are four *UVs* in total. Their amplitudes and directions are listed in Table V.

Similarly, universal virtual voltage vectors in remaining other small sectors can also be deduced. Ultimately, the whole modulation region of all universal virtual voltage vectors can span a range of 0–360° on the plane, as visually depicted in Fig. 22. Compared with Fig. 16(a), the universal voltage vectors choose to sacrifice part of the modulation area in exchange for wider application capability under different-phase faults. At this time, the maximum linear modulation index of universal virtual voltage vectors remains 0.7888, consistent with (21) under specific single open-switch fault.

D. Action Time Reallocation

After the universal virtual voltage vector is established, the next is to reallocate the action time of each voltage vector. The sector in which the reference voltage vector is located can be determined based on its angle

$$\theta_{sref} = \arctan\left(\frac{U_{\beta ref}}{U_{\alpha ref}}\right) \tag{22}$$

where θ_{sref} is the angle of reference voltage; $\boldsymbol{U}_{\alpha\beta\boldsymbol{ref}}$ is the reference voltage in α-β frame.

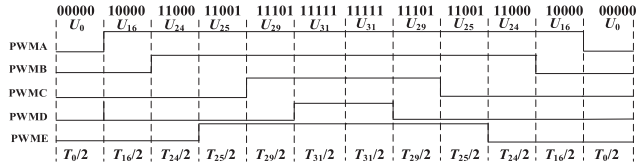

Fig. 23. Vector switching sequence and symmetrical PWM structure in small sector 2.

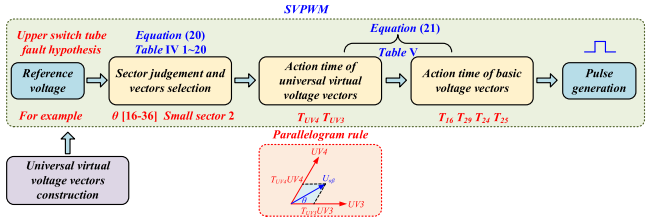

Fig. 24. Flowchart of universal fault-tolerant SVPWM strategy.

Assuming that the reference voltage vector is located in small sector 2, the action time of UV_3 and UV_4 can be determined according to the parallelogram rule. Furthermore, based on the action time ratio in Table IV, the action time of U_{16}, U_{25}, U_{29}, and U_{24} can be obtained as

$$\boldsymbol{U}_{\boldsymbol{\alpha\beta ref}} = T_{UV3}\boldsymbol{UV}_{3\alpha\beta} + T_{UV4}\boldsymbol{UV}_{4\alpha\beta}$$

$$\Rightarrow \begin{cases} T_{16} = 0.22T_{UV3}, T_{25} = 0.78T_{UV3} \\ T_{29} = 0.382T_{UV4}, T_{24} = 0.618T_{UV4} \\ T_0 = T_{31} = 0.5\left(1 - T_{16} - T_{25} - T_{29} - T_{24}\right) \end{cases} \tag{23}$$

where T_{UV3}, T_{UV4}, T_{16}, T_{25}, T_{29}, and T_{24} are the corresponding action time; T_0 and T_{31} are the action time of null vectors.

Since the serial number of the selected vector is consistent with that under normal conditions, the vector switching sequence and symmetrical PWM structure are still employed, which are shown in Fig. 23. The flowchart of proposed universal fault-tolerant SVPWM strategy is depicted in Fig. 24. The action time of *UVs* should be determined first, then the action time of basic voltage vectors can be resolved subsequently. The overall control block diagram of the control method is illustrated in Fig. 25. It should be emphasized that no changes of reference current and transformation matrix need to be considered. When designing the fault-tolerant strategy for five-phase motor, it is essential to mitigate the impact of the third harmonic subspace. By synthesizing virtual voltage vectors, the third harmonic voltage components can be reduced as much as possible. Therefore, the suppression of the third harmonic can be directly achieved within the SVPWM algorithm by minimizing the third harmonic voltage component of the voltage vectors. Furthermore, the closed-loop current control for both fundamental (d-q) and third harmonic (d_3-q_3) subspaces can be simplified to only fundamental (d-q) subspace, thereby reducing the complexity of the third harmonic current control structure in the system control

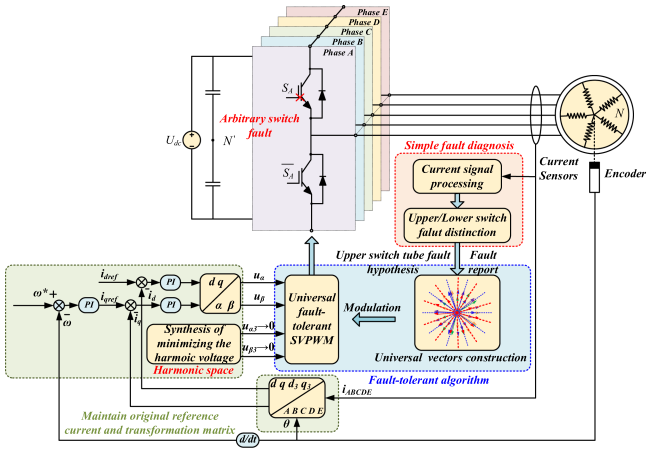

Fig. 25. Overall control block diagram of universal fault-tolerant SVPWM strategy with simplified fault diagnosis under arbitrary phase single open-switch fault.

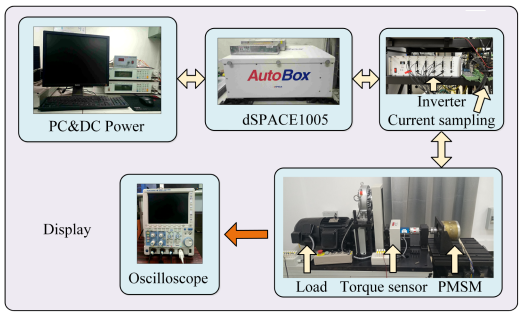

Fig. 26. Experimental platform.

TABLE VI
PRACTICAL PARAMETERS OF PROTOTYPE MOTOR

Parameter	Value
Number of pole pairs	4
Phase resistance	0.8 Ω
Fundamental d-axis inductance	5.3 mH
Fundamental q-axis inductance	17 mH
Leakage inductance	0.23 mH
Permanent magnet flux linkage	0.111 Wb
Rated speed	500 r/min

diagram. More importantly, the control method does not require excessive adjustments to handle different-phase open-switch faults.

VI. EXPERIMENT RESULTS

In order to validate the proposed fault tolerant control algorithm, an experimental platform has been established, as shown in Fig. 26. The test platform is based on a five-phase PMSM and its parameters are given in Table VI.

The proposed control method is developed and implemented in the dSPACE1005 controller and motor torque is measured by a high precision torque sensor (T20WN/20 Nm). The five-phase half-bridge inverter and current sampling module are also shown

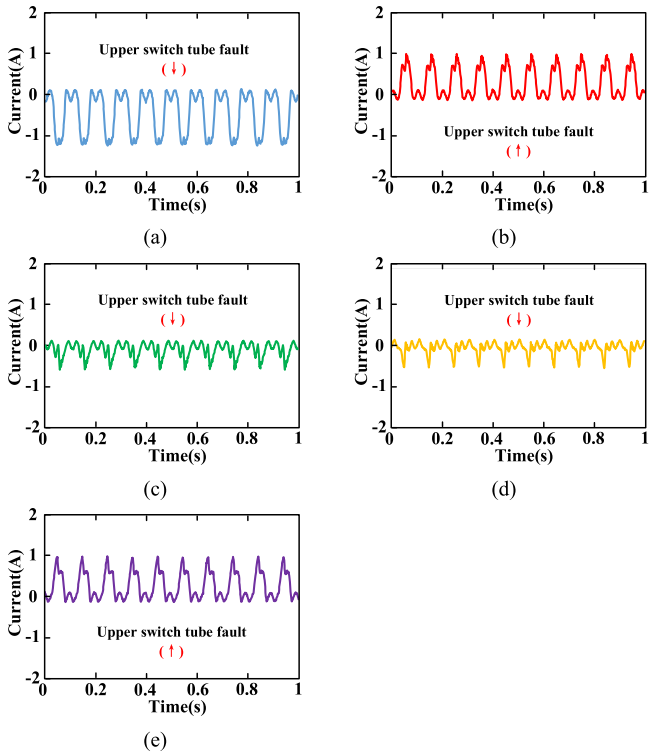

Fig. 27. Third harmonic components of five-phase currents under phase A upper switch tube fault (200 r/min). (a) Phase A. (b) Phase B. (c) Phase C. (d) Phase D. (e) Phase E.

in Fig. 26. In the experiment, open-switch fault is emulated by manually disconnecting PWM input signal.

A. Fault Diagnosis Test

The simplified open-switch fault diagnosis criteria are first verified. Taking phase A upper switch tube fault as an example, Figs. 27 and 28 show the corresponding third harmonic components of five-phase currents. Under a constant load torque of 2.6 Nm, two sets of experiments are operated at the speed of 200 r/min and 400 r/min, respectively.

As illustrated in Figs. 27 and 28, the third harmonic components under upper switch tube fault contain 3 (↓) and 2 (↑). "↑" represents that the third harmonic current is approximately greater than or equal to zero and "↓" represents the opposite. It can be concluded that positive and negative values of the third harmonic components are fully consistent with the analysis and simulation findings in Section III.

The third harmonic components of five-phase currents under all single open-switch fault conditions have been tallied and displayed in Table VII. The numbers of "↑" and "↓" under lower switch tube fault are the inverse of the numbers of "↑" and "↓" under upper switch tube fault. Then, the overall determination of upper or lower switch tube fault can be achieved based on the inverse relationship.

In order to completely validate the feasibility of fault diagnosis method, the average value of k in Fig. 9 is required application for practical experiments. Two sets of experiments are performed at 200 r/min and 400 r/min under a constant load torque of

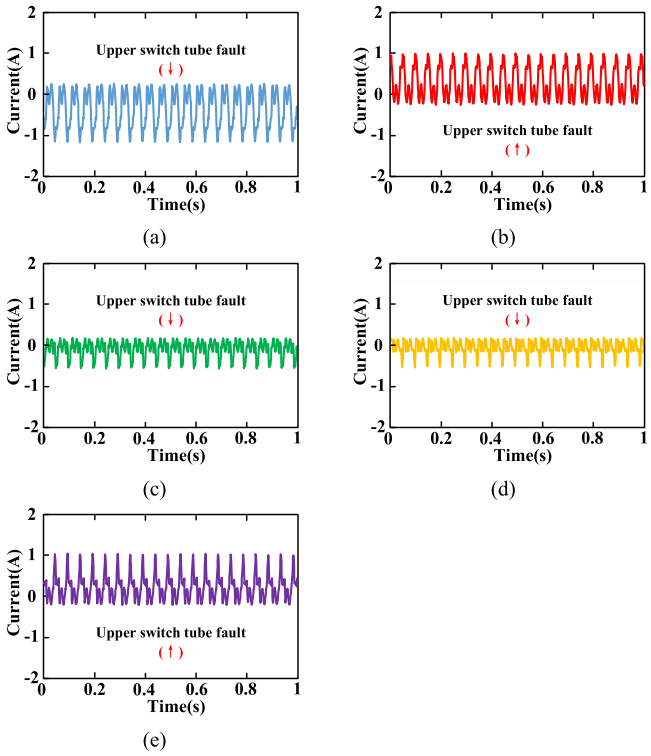

Fig. 28. Third harmonic components of five-phase currents under phase A upper switch tube fault (400 r/min). (a) Phase A. (b) Phase B. (c) Phase C. (d) Phase D. (e) Phase E.

TABLE VII
THIRD HARMONIC COMPONENTS OF FIVE-PHASE CURRENTS UNDER ALL SINGLE OPEN-SWITCH FAULT CONDITIONS

Phase	Tube	i_{A3}	i_{B3}	i_{C3}	i_{D3}	i_{E3}	Number(>0)	Number(<0)
A	upper	↓	↑	↓	↓	↑	2	3
	lower	↑	↓	↑	↑	↓	3	2
B	upper	↑	↓	↑	↓	↓	2	3
	lower	↓	↑	↓	↑	↑	3	2
C	upper	↓	↑	↓	↑	↓	2	3
	lower	↑	↓	↑	↓	↑	3	2
D	upper	↓	↓	↑	↓	↑	2	3
	lower	↑	↑	↓	↑	↓	3	2
E	upper	↑	↓	↓	↑	↓	2	3
	lower	↓	↑	↑	↓	↑	3	2

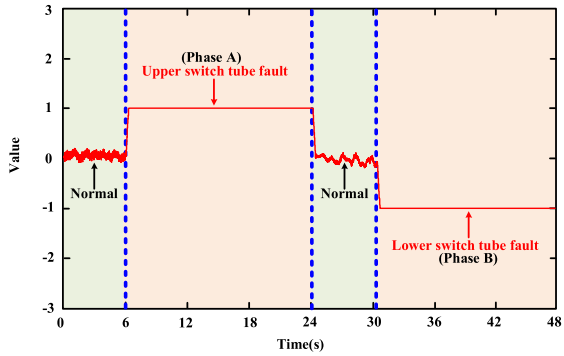

Fig. 29. Simplified fault diagnosis results from phase A upper switch tube fault to phase B lower switch tube fault (200 r/min).

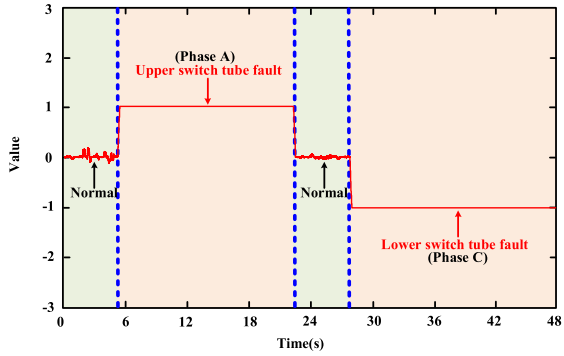

Fig. 30. Simplified fault diagnosis results from phase A upper switch tube fault to phase C lower switch tube fault (400 r/min).

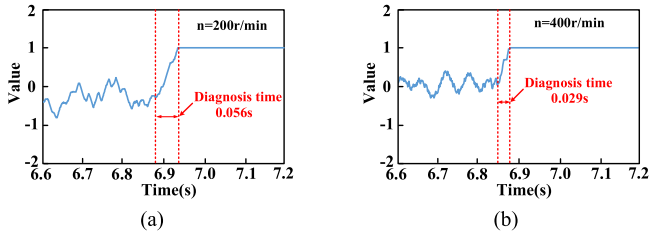

Fig. 31. Diagnosis time test from normal operation to phase A upper switch tube fault. (a) 200 r/min. (b) 400 r/min.

2.6 Nm. To simultaneously evaluate the universality of the proposed diagnosis method, fault condition selection includes phase A upper switch tube fault, phase B lower switch tube fault, and phase C lower switch tube fault. The simplified fault diagnosis results of open-switch faults under different locations are displayed in Figs. 29 and 30. When open-switch fault occurs, k value can quickly respond to it and tends to stabilize. The output k value presents either 1 or -1, corresponding to the upper or lower switch tube fault. Under normal conditions, the average value of k fluctuates around 0 due to accidental errors. Therefore, the simplified diagnosis method can effectively distinguish between normal condition, upper tube fault, and lower tube fault as a whole.

From Section III-B, it can be observed that the diagnosis time of the proposed method is influenced by the selection of T_m. Theoretically, a T_m value exceeding 0.5 electrical cycle is sufficient for diagnosis requirements. And, the electrical cycle varies linearly with the rotational speed. In the actual experimental process, T_m is set to 0.75 electrical cycle. Meanwhile, the diagnosis time of existing traditional methods usually ranges from 0.5 to 1 electrical cycle. From a theoretical perspective, the diagnosis time of the proposed method also falls within this range and meets the common standards.

Subsequently, the diagnosis time test is conducted on the proposed simplified diagnosis method. Similarly, two sets of experiments are performed at 200 r/min and 400 r/min in Fig. 31. Based on the motor parameters presented in Table VI, it can be inferred that the ideal diagnosis time range for the experimental motor in this article is within 0.0375 s to 0.075 s for 200 r/min and 0.01875 s to 0.0375 s for 400 r/min. As illustrated in Fig. 31, the diagnosis time is 0.056 s at 200 r/min

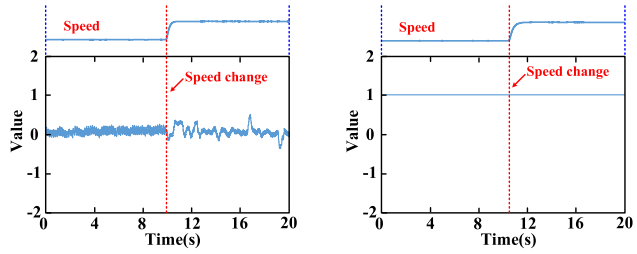

Fig. 32. Misdiagnosis test of k value under phase A upper switch tube fault (speed change). (a) Normal state ($-1<k<1$). (b) Fault state ($k=1$).

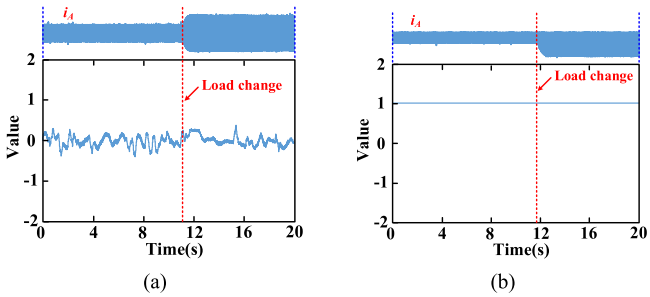

Fig. 33. Misdiagnosis test of k value under phase A upper switch tube fault (load change). (a) Normal state ($-1<k<1$). (b) Fault state ($k=1$).

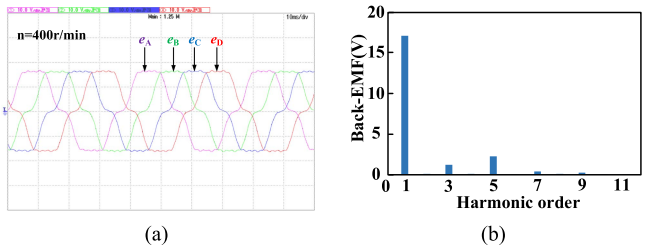

Fig. 34. Back EMF of the tested five-phase PMSM and its FFT analysis result. (a) Back EMF. (b) FFT analysis result.

and 0.029 s at 400 r/min. Overall, the response of the proposed simplified diagnosis method is very quick and satisfactory. Furthermore, with the increase in rotational speed, the diagnosis time decreases linearly, which is consistent with the theoretical analysis.

Finally, misdiagnosis test of the proposed method is presented. Since the proposed diagnosis approach does not rely on actual motor parameters, the factors of misdiagnosis test are defined as sudden changes in speed and load. Figs. 32 and 33 illustrate the variations in k value under speed change and load change, respectively, which include both normal state and fault state. Specifically, during the speed change, the load remains constant at 2.6 Nm while the speed increases from 100 to 400 r/min. Conversely, during the load change, the speed is maintained at 400 r/min while the load increases from 1.6 to 3 Nm. As illustrated in Figs. 32 and 33, the k value of diagnosis result remains stable under speed change and load change, without fluctuating into an erroneous state. It is precisely because the simplified diagnosis method only needs to differentiate between upper tube faults and lower tube faults as a whole that the k value of diagnosis result will only yield $k=1$ (upper tube fault), $k=-1$ (lower tube fault), or $-1<k<1$ (normal). The k-value waveform under normal state exhibits a wavy line ($\sim$) around 0, which distinctly contrasts with the straight line (-) in 1 or -1 of either upper tube fault or lower tube fault. In addition, the output of k value has also been processed by averaging in Fig. 9, which greatly avoids the influence of accidental errors. Hence, the proposed simplified diagnosis approach is almost free of misdiagnosis.

B. Fault-Tolerant Performance Test

Fig. 34 shows the back electromotive force (EMF) waveforms of the tested five-phase PMSM at a constant speed of 400 r/min. The experimental waveforms comprises back-EMFs of phase A, B, C, and D, and back EMF of phase A is specifically selected for FFT analysis. The amplitude of the back-EMF is 16.8 V and the waveform is approximately sinusoidal. As illustrated in Fig. 34(b), the fifth harmonic component accounts for 12.9%, which is the main harmonic back-EMF of the motor. But its effect on torque ripple is mitigated due to the star connection of the windings. Although the third harmonic back-EMF can produce torque ripple when reacting with the fundamental current, it only accounts for 6.3% and is relatively small. Hence, the tested PMSM can be approximately defined as a standard five-phase motor with sinusoidal back EMF.

After diagnosing the switch tube fault in Section VI-A, the fault-tolerance performance of the proposed universal SVPWM strategy is subsequently validated. The assumption made here is that the diagnosis indicates an upper switch tube fault. In order to exhibit the universality of fault-tolerant method, the proposed universal method does not change under different-phase open-switch fault. Fig. 35 Shows the phase currents and torque waveforms around the fault occurrence. The motor is operated at a constant speed of 380 r/min and the load torque is 2.9 Nm. Fig. 35(a)–(e) are, respectively, the processes from normal operation to fault and fault-tolerant operation under phase A, B, C, D, and E upper switch tube fault. On one hand, it can be seen that the proposed method can significantly mitigate the torque ripple induced by the switch tube fault. Specifically, the torque ripples can be reduced from 134%–135% to 41%–42% after the application of fault-tolerant algorithm, which is close to 21% under normal operation. On the other hand, the proposed method does not require readjustment based on the change of faulty phase. It can be universally applied to different-phase switch tube faults, which is more versatile and convenient.

In order to provide a clearer and more intuitive analysis on torque performance, FFT analysis is conducted separately on the torque from Fig. 35. The torque under phase A, B, and C upper tube fault conditions are selected as analysis objects. The corresponding results are depicted in Fig. 36. It can be concluded that the application of the proposed fault-tolerant method effectively mitigates the dominant harmonic components of torque during switch tube faults. The torque ripple of the first, second and third order, respectively, decreases from approximately 1.2 Nm,

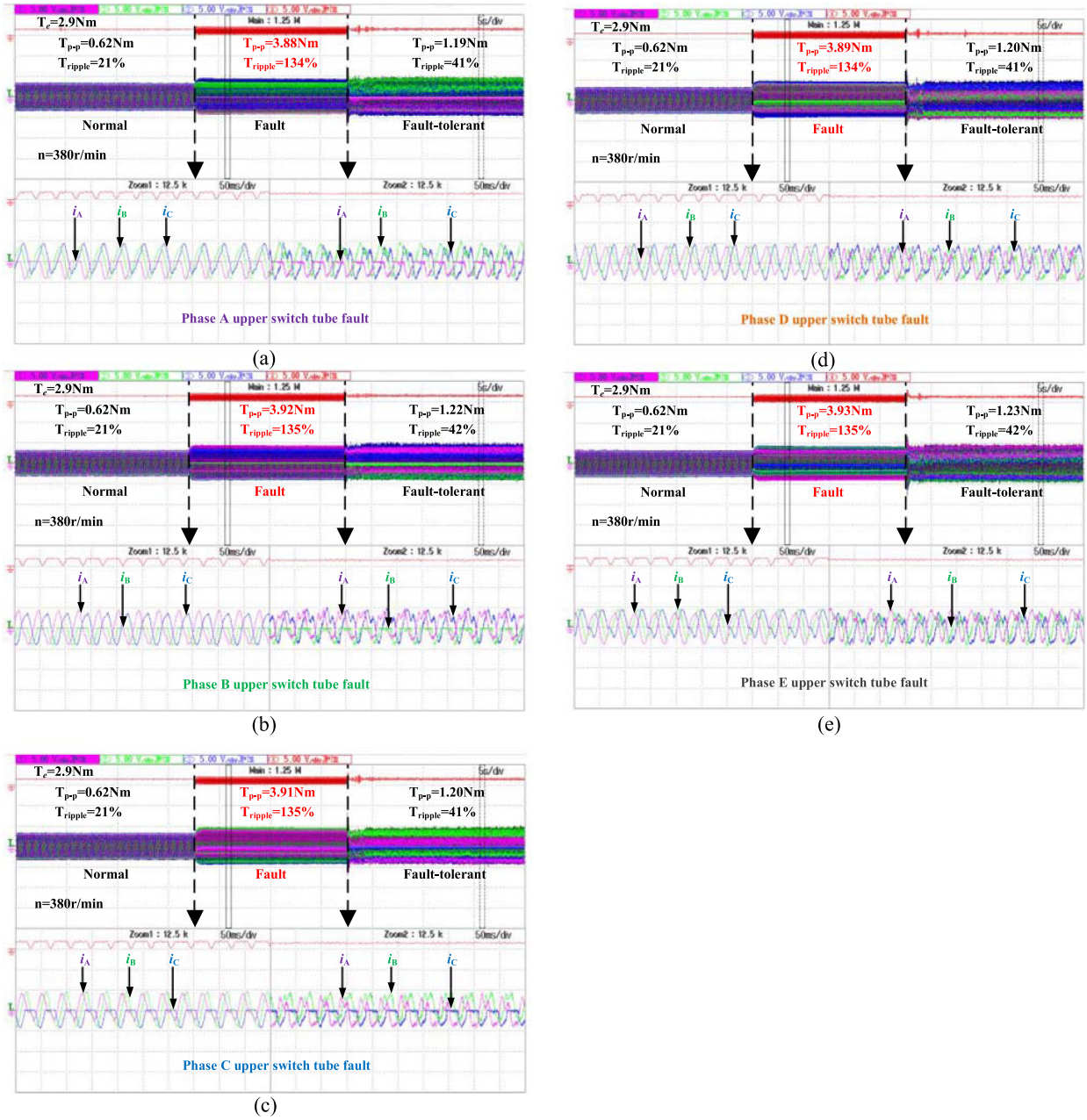

Fig. 35. Torque and currents waveforms from normal operation to fault and fault-tolerant operation. (a) Phase A upper switch tube fault. (b) Phase B upper switch tube fault. (c) Phase C upper switch tube fault. (d) Phase D upper switch tube fault. (e) Phase E upper switch tube fault. *Te* is scaled to 10 Nm/div, phase currents are scaled to 5 A/div.

0.8 Nm, and 0.5 Nm to below 0.2 Nm, which result in a satisfied torque quality that closely resembles normal motor operation.

The torque of five-phase PMSM can be expressed as

$$T_e = \frac{5}{2} p \left[\left(L_d - L_q \right) i_d i_q + i_q \varphi_f \right] \tag{24}$$

where p is the pole pairs; i_d, i_q are the d-q axes currents; L_d, L_q are the d-q axes inductances; φ_f is the permanent magnet flux linkage.

It is obvious from (24) that torque ripples are primarily attributed to the fluctuation of d-q axes currents. Taking phase A upper switch tube as an example, Fig. 37 shows the d-q axes currents from normal operation to fault and fault-tolerant operation. When open-switch fault occurs, d-q axes currents exhibit significant fluctuations. After the implementation of proposed fault-tolerant algorithm, the current fluctuations have been substantially mitigated. This behavior is consistent with the observed performance of the torque.

Therefore, from the aspects of both torque and d-q axes current, the proposed method makes the motor still remain good steady-state performance in case of open-switch fault. To highlight the universality of the proposed fault-tolerant method, Fig. 38 presents a comparison between the proposed general fault-tolerant approach and traditional specific fault-tolerant

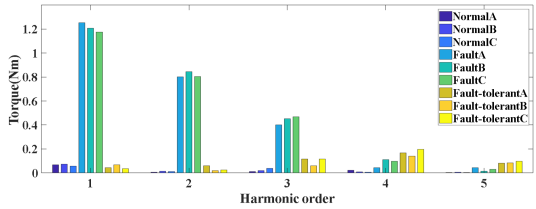

Fig. 36. FFT analysis results of torque under different operations.

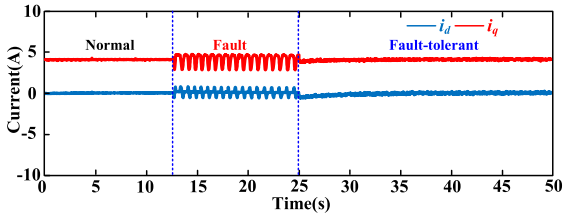

Fig. 37. *d-q* axes currents from normal operation to fault and fault-tolerant operation (phase A upper switch tube fault).

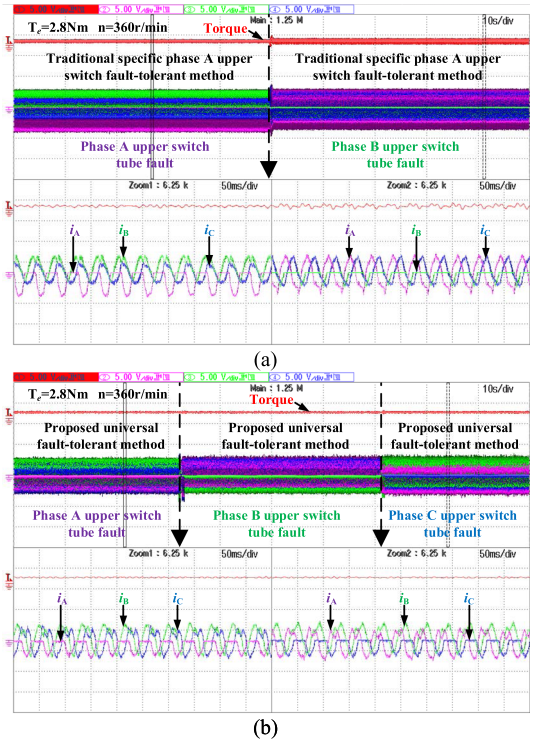

Fig. 38. Comparison on the universality of fault-tolerant methods under different-phase open-switch faults. (a) Traditional specific phase A upper switch fault-tolerant method in [21]. (b) Proposed universal fault-tolerant method. *Te* is scaled to 10 Nm/div, phase currents are scaled to 5 A/div.

method. The motor is operated at a constant speed of 360 r/min and the load torque is 2.8 Nm. Taking the method in [21] as an example, this method is a fault-tolerant strategy proposed only for phase A upper tube fault. As illustrated in Fig. 38(a), when this specific strategy is applied to phase A upper tube fault, it results in increased torque ripples. This indicates that

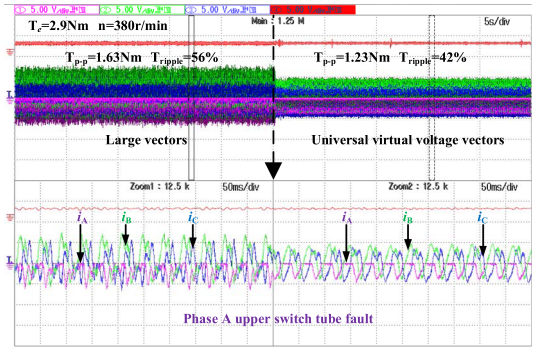

Fig. 39. Comparison of the proposed universal virtual voltage vector method against an algorithm without virtual voltage vector synthesis. *Te* is scaled to 10 Nm/div, phase currents are scaled to 5 A/div.

traditional fault-tolerant strategies are limited to handling open-switch fault in a sole predefined specific phase. When transitioning to other noncorresponding phases, traditional specific methods are unable to maintain the original performance, and additional disturbances arise. Even during the switching process, significant jitter also occurs. In contrast, Fig. 38(b) illustrates the switching process of the proposed universal fault-tolerant method, transitioning from phase A upper tube fault to phase B upper tube fault and phase C upper tube fault sequentially. This method is applicable to open-switch faults located in different phases, and the transition process is notably smooth. The torque ripple remains consistently low, indicating strong stability and excellent universality.

To validate the effectiveness of the virtual voltage vector in suppressing third harmonics, the proposed universal virtual voltage vector method is compared against an algorithm that does not employ virtual voltage vector synthesis. As shown in Fig. 39, the motor is operated at a constant speed of 380 r/min and the load torque is 2.9 Nm under phase A upper switch tube fault. The algorithm presented on the left utilizes the ten large vectors derived in Fig. 11, whereas the approach on the right employs the proposed universal virtual voltage vector method. After the implementation of the virtual voltage vector synthesis, the torque ripple is reduced from 56% to 42% compared to the algorithm that solely employs the reconstructed large vectors. Additionally, the fluctuation in phase current is also notably diminished. Fig. 40 illustrates the comparison of d_3-q_3 axes currents for the two algorithms. Compared to the large vectors, the virtual voltage vectors reduce the third harmonic voltage components in α_3-β_3 subspace by synthesizing two voltage vectors. The voltage synthesis in α_3-β_3 subspace will be mapped onto the suppression of d_3-q_3 axes currents. As illustrated in Fig. 40(a) and (b), the fluctuations of d_3-q_3 axes currents are effectively diminished after transitioning from utilizing large vectors to utilizing universal virtual voltage vectors. As can be observed from the further comparison presented in Fig. 40(c)–(e), the amplitudes of d_3-q_3 axes with the synthesis of the third harmonic voltage is significantly lower than that without such synthesis. The fluctuation of the amplitude is approximately within 1 A, which is acceptable. Hence, the

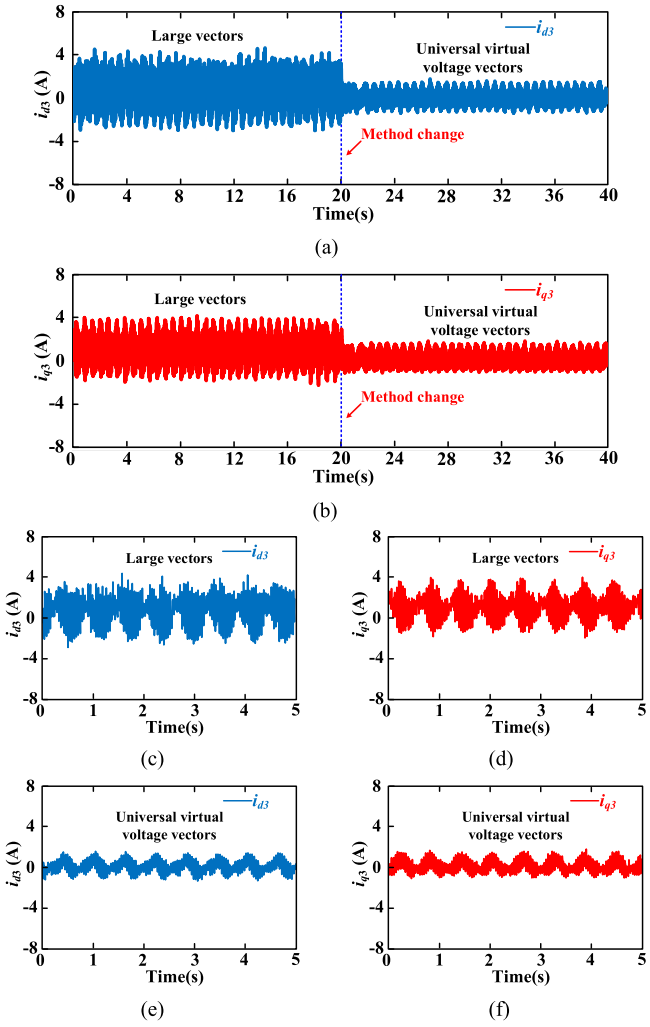

Fig. 40. Comparison of d_3-q_3 axes currents under phase A upper switch tube fault. (a) Switching process of d_3-axis current. (b) Switching process of q_3-axis current. (c) d_3-axis current (large vectors). (d) q_3-axis current (large vectors). (e) d_3-axis current (universal virtual voltage vectors). (f) q_3-axis current (universal virtual voltage vectors).

proposed universal virtual voltage vector method can effectively suppress third harmonics.

C. Dynamic Performance Test

To evaluate the dynamic response of the proposed fault-tolerant method, speed change, and load change tests should be, respectively, performed. Due to the symmetrical structure of the five-phase motor, only phase A upper switch tube fault is selected for example and demonstration. Fig. 41 shows experimental speed, torque, and current responses under a speed change. The torque is set at 2.9 Nm and the speed is varied from 120 to 360 r/min. The speed tracking is satisfactorily achieved with a fast response and low overshoot.

Fig. 42 shows a test to further verify that the proposed strategy maintains a high performance and robustness in terms of load step. The motor is driven in steady state with constant speed of

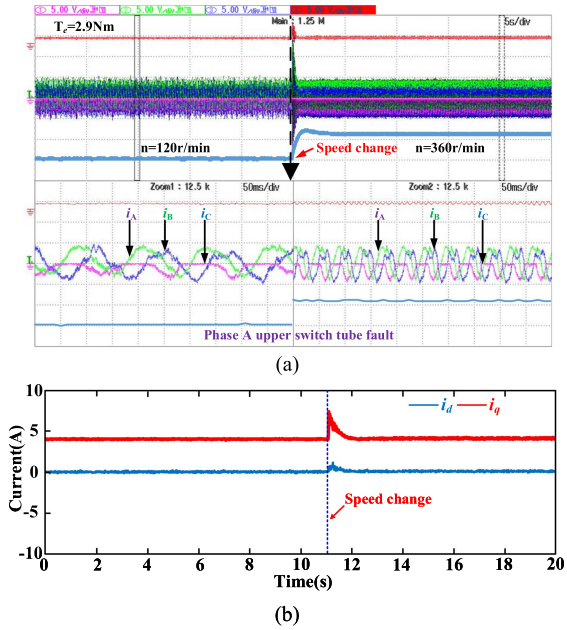

Fig. 41. Speed, torque, and current responses under a speed change. (a) Speed, torque and phase currents (*Te* is scaled to 10 Nm/div, phase currents are scaled to 5 A/div). (b) *d*-*q* axes currents.

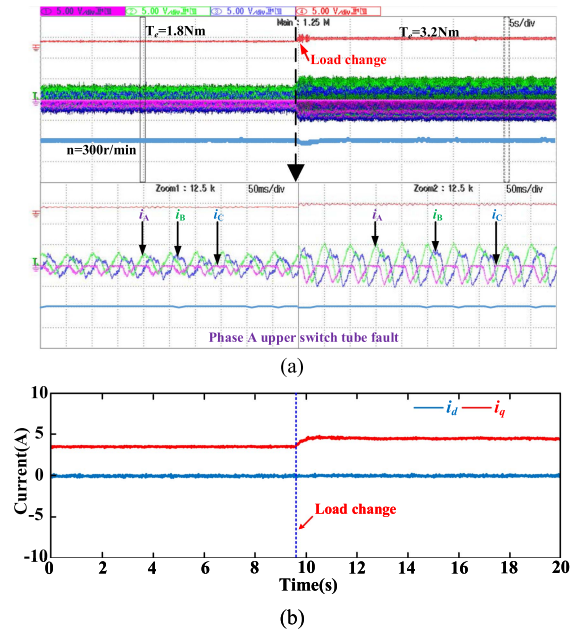

Fig. 42. Speed, torque, and current responses under a load change. (a) Speed, torque, and phase currents (*Te* is scaled to 10 Nm/div, phase currents are scaled to 5 A/div). (b) *d*-*q* axes currents.

300 r/min. The load is varied from 1.8 to 3.2 Nm. Also torque and currents can track the given reference value. Consequently, the proposed method can provide fast dynamic response and low overshoot in the face of speed and load sudden changes. In addition, under different speed and load conditions, the motor can all effectively maintain satisfactory operating characteristics.

VII. Conclusion

This article proposes a universal fault-tolerant SVPWM strategy with simplified fault diagnosis to realize arbitrary phase single open-switch fault-tolerant operation for five-phase PMSM. The simplified open-switch diagnosis necessitates only an overall assessment of the upper or lower tube, thereby reducing the diagnosis states and computation burden. Then, the universal fault-tolerant SVPWM strategy can realize fault-tolerant operation without the need for readjustment based on the fault phase location. The experimental results show that the simplified diagnostic method can effectively distinguish between normal condition, upper tube fault and lower tube fault as a whole. When switch tube fault located in different phases occurs, the universal fault-tolerant SVPWM strategy can significantly mitigate the torque ripple without readjustment based on the change of faulty phase. In addition, the proposed method can still maintain satisfactory dynamic performance in the face of speed and load sudden changes.

In future research, we will explore occasions involving multiple switch tube faults and the influence of third harmonic back EMF to broaden the applicability of diagnosis methods and fault-tolerant strategies. Furthermore, we will continue to enhance the torque and current performance under fault-tolerant operation.

References

[1] T. Zhao, S. Wu, and S. Cui, "Multiphase PMSM with asymmetric windings for more electric aircraft," *IEEE Trans. Transp. Electrific.*, vol. 6, no. 4, pp. 1592–1602, Dec. 2020.

[2] R. Huang, Z. Dong, B. Zhang, and C. Liu, "Decoupled modulation strategy for harmonic current suppression in five-phase series-end winding PMSM drives," *IEEE Trans. Ind. Electron.*, vol. 71, no. 10, pp. 13480–13485, Oct. 2024, doi: 10.1109/TIE.2024.3349582.

[3] S. Yang, P. Zheng, Y. Sui, C. Tong, and M. Wang, "Carrier-based PWM technique and extended state observer-based current control scheme for current-source inverter-fed five-phase PMSM drives," *IEEE Trans. Ind. Electron.*, vol. 71, no. 7, pp. 6635–6646, Jul. 2024, doi: 10.1109/TIE.2023.3301518.

[4] C. Jiang, H. Liu, P. Wheeler, F. Wu, and J. Huo, "An optimized modulation for five-phase open-end winding PMSM with sliding clamped strategy," *IEEE Trans. Ind. Electron.*, vol. 70, no. 9, pp. 8819–8829, Sep. 2023, doi: 10.1109/TIE.2022.3212385.

[5] H. Wang et al., "Fault-tolerant control for single-phase open-circuit and short-circuit fault in five-phase PMSM with third-order harmonic back EMF using coefficients reconfiguration," *IEEE Trans. Energy Convers.*, vol. 39, no. 1, pp. 782–792, Mar. 2024.

[6] S. Yang, C. Tong, Y. Sui, Z. Yin, and P. Zheng, "Current-source inverter fed five-phase PMSM drives with pentagon stator winding considering SVM scheme, resonance damping, and fault tolerance," *IEEE Trans. Ind. Electron.*, vol. 70, no. 6, pp. 5560–5570, Jun. 2023, doi: 10.1109/TIE.2022.3190848.

[7] S. Yang, P. Zheng, Y. Sui, C. Tong, and M. Wang, "Open-circuit fault-tolerant control for pentagon winding connected five-phase current-source inverter based PMSM drives," *IEEE Trans. Ind. Electron.*, vol. 71, no. 3, pp. 2277–2288, Mar. 2024.

[8] C. Xiong, T. Guan, P. Zhou, and H. Xu, "A Fault-tolerant FOC strategy for five-phase SPMSM with minimum torque ripples in the full torque operation range under double-phase open-circuit fault," *IEEE Trans. Ind. Electron.*, vol. 67, no. 11, pp. 9059–9072, Nov. 2020, doi: 10.1109/TIE.2019.2950851.

[9] B. Tian, J. Wei, M. Molinas, R. Lu, Q. An, and B. Zhou, "Neutral voltage modeling and its remediation for five-phase PMSMs under single-phase short-circuit fault tolerant control," *IEEE Trans. Transp. Electrific.*, vol. 8, no. 4, pp. 4534–4548, Dec. 2022.

[10] Z. Yin, Y. Sui, P. Zheng, S. Yang, Z. Zheng, and J. Huang, "Short-circuit fault-tolerant control without constraint on the d-axis armature magnetomotive force for five-phase PMSM," *IEEE Trans. Ind. Electron.*, vol. 69, no. 5, pp. 4472–4483, May 2022, doi: 10.1109/TIE.2021.3084172.

[11] W. Fang, B. Zhou, K. Wang, Y. Zhang, and J. Wei, "A fault diagnosis and fault-tolerant control method for open-switch faults of converters in DSEM drive system," *IEEE Trans. Ind. Electron.*, vol. 71, no. 8, pp. 8459–8470, Aug. 2024.

[12] R. Cui and Y. Fan, "A new fault-tolerant control strategy for open-winding drive system under single leg open-circuit fault," in *Proc. 21st Int. Conf. Elect. Mach. Syst.*, 2018, pp. 1492–1497, doi: 10.23919/ICEMS.2018.8549085.

[13] W. Zhao, B. Wu, Q. Chen, and J. Zhu, "Fault-tolerant direct thrust force control for a dual inverter fed open-end winding linear vernier permanent-magnet motor using improved SVPWM," *IEEE Trans. Ind. Electron.*, vol. 65, no. 9, pp. 7458–7467, Sep. 2018.

[14] Y. Zuo, X. Zhu, X. Si, and C. H. T. Lee, "Fault-tolerant control for multiple open-leg faults in open-end winding permanent magnet synchronous motor system based on winding reconnection," *IEEE Trans. Power Electron.*, vol. 36, no. 5, pp. 6068–6078, May 2021.

[15] Y. Du, T. Tao, X. Zhao, W. Zhao, J. Ji, and Z. Li, "Inverter reconstruction approach for open-end winding five-phase PMSM with pattern-based vector synthesis and hybrid SVPWM modulation," *IEEE Trans. Power Electron.*, vol. 39, no. 10, pp. 13597–13612, Oct. 2024, doi: 10.1109/TPEL.2024.3422218.

[16] G. Li, Q. Zhu, B. Li, Y. Zhao, and X. Ma, "Open-circuit fault-tolerant vector control for five-phase SPMSM based on five-phase six-leg inverter," *IEEE Trans. Energy Convers.*, vol. 38, no. 1, pp. 404–416, Mar. 2023.

[17] H. Zhou, W. Zhao, G. Liu, R. Cheng, and Y. Xie, "Remedial field-oriented control of five-phase fault-tolerant permanent-magnet motor by using reduced-order transformation matrices," *IEEE Trans. Ind. Electron.*, vol. 64, no. 1, pp. 169–178, Jan. 2017.

[18] B. Tian, Q.-T. An, J.-D. Duan, D.-Y. Sun, L. Sun, and D. Semenov, "Decoupled modeling and nonlinear speed control for five-phase PM motor under single-phase open fault," *IEEE Trans. Power Electron.*, vol. 32, no. 7, pp. 5473–5486, Jul. 2017.

[19] B. Tian, M. Molinas, Q. An, B. Zhou, and J. Wei, "Freewheeling current-based sensorless field-oriented control of five-phase permanent magnet synchronous motors under insulated gate bipolar transistor failures of a single phase," *IEEE Trans. Ind. Electron.*, vol. 69, no. 1, pp. 213–224, Jan. 2022.

[20] J. Sun, Z. Zheng, C. Li, K. Wang, and Y. Li, "Optimal fault-tolerant control of multiphase drives under open-phase/open-switch faults based on DC current injection," *IEEE Trans. Power Electron.*, vol. 37, no. 5, pp. 5928–5936, May 2022.

[21] W. Huang, X. Zhu, H. Zhang, and W. Hua, "Generalized fault-tolerant model predictive control of five-phase PMSM drives under single/two open-switch faults," *IEEE Trans. Ind. Electron.*, vol. 70, no. 8, pp. 7569–7579, Aug. 2023.

[22] Z. Zhang, Y. Hu, G. Luo, C. Gong, X. Liu, and S. Chen, "An embedded fault-tolerant control method for single open-switch faults in standard PMSM drives," *IEEE Trans. Power Electron.*, vol. 37, no. 7, pp. 8476–8487, Jul. 2022.

[23] W. Huang et al., "Current-based open-circuit fault diagnosis for PMSM drives with model predictive control," *IEEE Trans. Power Electron.*, vol. 36, no. 9, pp. 10695–10704, Sep. 2021, doi: 10.1109/TPEL.2021.3061448.

[24] B. Wang, X. Feng, T. Sun, Z. Wang, and M. Cheng, "Relative β-axis residual voltage signal based fault detection for inverter switch open-circuit failure," *IEEE Trans. Power Electron.*, vol. 38, no. 9, pp. 11315–11326, Sep. 2023.

[25] Z. Wu, W. Hua, C. Cheng, and J. Du, "Robust sensorless strategy for dual three-phase PMSM by the virtual EMF under single open-phase/open-switch fault," *IEEE Trans. Ind. Electron.*, vol. 72, no. 1, pp. 49–59, Jan. 2025, doi: 10.1109/TIE.2024.3406852.

[26] G. Yang, H. Hussain, S. Li, X. Zhang, J. Yang, and C. H. T. Lee, "Design and analysis of universal natural fault-tolerant SVPWM strategy with simplified fault diagnosis for multiphase motor drives," *IEEE Trans. Emerg. Sel. Topics Power Electron.*, vol. 11, no. 4, pp. 4340–4354, Aug. 2023.

[27] H. Zhou, C. Chen, X. Xiang, and G. Liu, "Switching-table-based diagnosis-free fault-tolerant DTC for five-phase PMSM with any phase open-circuit fault," *IEEE Trans. Ind. Electron.*, vol. 71, no. 11, pp. 13790–13800, Nov. 2024.

Xu Wang (Member, IEEE) received the B.Sc. degree in electrical automation in 2019 from Jiangsu University, Zhenjiang, China, where he is currently working toward the Ph.D. degree in control science and engineering.

His research interests include model predictive control of electric machines and fault-tolerant control.

Zhengmeng Liu (Member, IEEE) received the B.S. degree from Chongqing University, Chongqing, China, in 2013, the M.S. degree from Jiangsu University, Zhenjiang, China, in 2016, and the Ph.D. degree from the University of Sheffield, Sheffield, U.K., in 2021, all in electrical engineering.

He has been with Jiangsu University since 2021, where he is currently a Lecturer with the School of Electrical Information Engineering. His research interests include the design, control, and analysis of permanent magnet electrical machines and linear actuators.

Qian Chen (Senior Member, IEEE) received the B.Sc. and Ph.D. degrees from Jiangsu University, Zhenjiang, China, in 2009 and 2015, respectively, both in electrical engineering and control engineering.

He has been with Jiangsu University since 2015, where he is currently an Associate Professor with the School of Electrical Information Engineering. He is a Full Member of Sigma Xi, The Scientific Research Honor Society. From 2020 to 2021, he was a Visiting Professor with the Department of Electronic and Electrical Engineering, University of Sheffield, Sheffield, U.K. His current research interests include electric machine design, modeling, fault analysis, and intelligent control.

Wenxiang Zhao (Senior Member, IEEE) received the B.Sc. and M.Sc. degrees in electrical engineering from Jiangsu University, Zhenjiang, China, in 1999 and 2003, respectively, and the Ph.D. degree in electrical engineering from Southeast University, Nanjing, China, in 2010.

From 2008 to 2009, he was a Research Assistant with the Department of Electrical and Electronic Engineering, University of Hong Kong, Hong Kong. From 2013 to 2014, he was a Visiting Professor with the Department of Electronic and Electrical Engineering, University of Sheffield, Sheffield, U.K. He is currently a Professor with the School of Electric Power Engineering, Nanjing Institute of Technology, and also with School of School of Electrical and Information Engineering, Jiangsu University. He has authored and coauthored more than 150 papers published in various IEEE Transactions. His current research interests include electric machines and control.

Guohai Liu (Senior Member, IEEE) received the B.Sc. degree from Jiangsu University, Zhenjiang, China, in 1985, and the M.Sc. and Ph.D. degrees from Southeast University, Nanjing, China, in 1988 and 2002, respectively, all in electrical engineering and control engineering.

Since 1988, he has been with the Jiangsu University, where since 2002, he has been a Professor with the School of Electrical Information Engineering. He is currently the Director with the Jiangsu Key Laboratory of Drive and Intelligent Control for Electric Vehicle. From 2003 to 2004, he was a Visiting Professor with the Department of Electronic and Electrical Engineering, University of Sheffield, Sheffield, U.K. He has authored or coauthored more than 300 technical papers and 4 textbooks, and is the holder of 80 patents in these areas. His teaching and research interests include electrical machines, motor drives for EV, and intelligent control.

Prof. Liu is a Fellow of Institution of Engineering and Technology, U.K.